Ecological Informatics 85 (2025) 102986

Contents lists available at ScienceDirect

Ecological Informatics

journal homepage: www.elsevier.com/locate/ecolinf

Spatiotemporal analysis of surface Urban Heat Island intensity and the role of vegetation in six major Pakistani cities

Shoaib Ahmad Anees[a,*,1], Kaleem Mehmood[b,c,d,1], Syed Imran Haider Raza[e], Sebastian Pfautsch[f], Munawar Shah[g], Punyawi Jamjareegulgarn[h], Fahad Shahzad[i], Abdullah A. Alarfaj[j], Sulaiman Ali Alharbi[j], Waseem Razzaq Khan[k,*], Timothy Dube[l]

[a] *Department of Forestry, The University of Agriculture, Dera Ismail Khan 29050, Pakistan*
[b] *College of Forestry, Beijing Forestry University, Beijing 100083, PR China*
[c] *Institute of Forest Science, University of Swat, Main Campus Charbagh, 19120 Swat, Pakistan*
[d] *Key Laboratory for Silviculture and Conservation of Ministry of Education, Beijing Forestry University, Beijing 100083, PR China*
[e] *Punjab Forest Department, Lahore, Pakistan*
[f] *Urban Transformations Research Centre, Western Sydney University, Parramatta, NSW 2150, Australia*
[g] *Department of Space Science, Institute of Space Technology, Islamabad 44000, Pakistan*
[h] *King Mongkut's Institute of Technology Ladkrabang, Prince of Chumphon Campus, Chumphon 86160, Thailand*
[i] *Mapping and 3S Technology Center, Beijing Forestry University, Beijing 100083, China*
[j] *Department of Botany and Microbiology, College of Science, King Saud University, P. O. Box. 2455, Riyadh 11451, Saudi Arabia*
[k] *Department of Forestry Science and Biodiversity, Faculty of Forestry and Environment, Universiti Putra Malaysia UPM, Serdang 43400, Selangor, Malaysia*
[l] *Institute for Water Studies, Faculty of Science, University of the Western Cape, Cape Town, South Africa*

ARTICLE INFO

Keywords:
Urban Heat Island
Remote sensing
Urban expansion
Vegetation cover
Climate change mitigation

ABSTRACT

The Urban Heat Island (UHI) phenomenon exacerbates thermal discomfort in urban areas and significantly contributes to urban overheating when combined with climate change. This study investigates the spatiotemporal patterns of Surface Urban Heat Island Intensity (SUHII) in six major cities of Pakistan, focusing on the interplay between urban expansion, vegetation cover, and SUHII. To quantify SUHII dynamics, the impact of urban sprawl and vegetation changes was analyzed. The study offers critical insights into the implications for urban planning and policymaking in Pakistan. Using remote sensing data from Landsat satellites, analyzed with Geographic Information Systems (GIS) techniques, estimates of SUHII, urban expansion, and vegetation cover were derived. Specifically, imagery from Landsat-5 (2010–2013) and Landsat-8 (2014–2022), obtained from the US Geological Survey (USGS), was employed. Statistical analyses, including Pearson's correlation and linear regression, were conducted to assess relationships between these variables from 2010 to 2022. **SUHII** was found to increase annually by 0.18 °C in Islamabad and 0.19 °C in Peshawar, with corresponding urban expansion rates of 8.07 km^2 (8967.75 pixels) and 1.67 km^2 (1860.42 pixels) per year, respectively. Vegetation indices such as the Normalized Difference Vegetation Index (NDVI) and Fractional Vegetation Cover (FVC) were inversely correlated with SUHII, explaining up to 50 % of the variance in Peshawar. However, weaker correlations in Lahore suggest the presence of additional factors influencing **SUHII**. A distinct spatial relationship between increased vegetation and cooler areas was observed. For instance, Islamabad has greater vegetation cover and cool zones over 41.5 km^2. In contrast, Lahore's hot spots spanned 127.1 km^2, compared to Abbottabad's 10.4 km^2, underscoring the thermal impact of reduced vegetation. The findings emphasize the effectiveness of urban greening, particularly in Islamabad's neutral thermal regions, in mitigating **SUHII**. This study offers important insights for urban planners in developing sustainable, climate-resilient cities within similar urban contexts. While the results are specific to Pakistani cities, the role of vegetation in mitigating **SUHII** may hold broader relevance for urban planning strategies in comparable settings.

* Corresponding authors.
E-mail addresses: anees.shoaib@gmail.com (S.A. Anees), khanwaseem@upm.edu.my (W.R. Khan).
[1] These authors contributed equally to this work.

https://doi.org/10.1016/j.ecoinf.2024.102986
Received 18 February 2024; Received in revised form 29 December 2024; Accepted 29 December 2024
Available online 30 December 2024
1574-9541/

1. Introduction

The world's population is expected to increase from its present estimate of 8 billion people (Haris et al., 2023) to 9 billion people by around 2037 (Pison, 2022). Urban climate conditions are expected to be significantly impacted by this demographic expansion. Despite its relatively small geographic scope, urbanization has a significant impact on surface energy, water, and carbon budgets (Haider et al., 2017; Jallat et al., 2021), as well as surface climate (Khan et al., 2020). Urban ambient temperatures are generally more important than those in rural regions due to changes in surface qualities, such as installing impermeable pavements and increased heat output from human activity (Bounoua et al., 2015). SUHII Effect is a widely used term for this climatic discrepancy (Soltani and Sharifi, 2019).

Additionally, research has demonstrated that planned urban growth can result in less warming than unplanned urban expansion (Khan et al., 2024; Zhou et al., 2019). Future urban temperatures can be significantly influenced by the interaction of urbanization and climate change, underscoring the significance of considering both the current characteristics of our cities and the extent of future urbanization (Yang et al., 2016). Numerous adverse effects have been connected to the well-documented SUHII. These include increased energy use, increased greenhouse gas emissions (Allam, 2021), adverse health effects (Huang et al., 2020a), reduced water quality (Koomen and Diogo, 2017), worsened local air pollution (Piracha and Chaudhary, 2022), and a rise in the frequency of extreme weather events, all of which could exacerbate the broader effects of urban overheating (Soltani and Sharifi, 2019).

SUHII are evaluated through remote sensing techniques and meteorological data, offering unique perspectives on urban thermal dynamics. Remote sensing captures the thermal characteristics of metropolitan areas from satellite observations, providing a broad view of spatial and temporal temperature variations (Huang et al., 2020b; Stewart et al., 2021). These satellite-based observations are crucial for understanding how urban expansion and vegetation loss contribute to rising surface temperatures (Chen et al., 2022; Zhang et al., 2024a). Remote sensing's extensive spatial coverage and cost-effectiveness have made it a preferred method for monitoring SUHI globally (Wang et al., 2023). Tools such as the Enhanced Thematic Mapper Plus (ETM+) and Landsat Thematic Mapper (TM) have provided invaluable insights into the temporal trends of SUHII across entire cities (Zhou et al., 2019). These studies have provided evidence of intensifying or expanding SUHII in several Pakistani cities, including Rawalpindi, Gujranwala, Lahore, Karachi, and Hyderabad, with the Covid-19 pandemic potentially influencing these patterns. During the pandemic, reduced human activity, such as decreased transportation and industrial operations, may have temporarily lowered heat emissions, leading to observable changes in SUHII (Aslam et al., 2021; Xu et al., 2022).

Multiple factors, including urban configuration, surface materials, and anthropogenic heat emissions, influence urban areas' thermal responses. These characteristics impact near-surface air temperatures and surface temperatures differently, making it challenging to predict UHI dynamics from one method alone (Scolio et al., 2024; Xiang et al., 2023; Zhang et al., 2024b). Urban green infrastructure, such as trees and lawns, helps mitigate rising temperatures, while grey infrastructure, like buildings and roads, contributes to warming. Changes in surface properties and land use can thus be effectively traced by analyzing spatio-temporal shifts in SUHII using remote sensing data.

The utilization of MODIS (Moderate Resolution Imaging Spectroradiometer) land surface temperature (LST) data has gained significant traction in the investigation of the spatial and temporal fluctuations of SUHII at both regional and global scales (Monteiro et al., 2021; Wu et al., 2019). It is well established that vegetation cover is a significant determinant of SUHII, as evidenced by several vegetation indices, including the NDVI, Enhanced Vegetation Index (EVI), and (Fractional Vegetation Cover Index (FVCI) (e.g., Flores et al., 2016; Mathew et al., 2015; Zhu et al., 2016). While impermeable surfaces exert the most significant influence on the intensity of the SUHII (Chen et al., 2019), vegetation has been observed to partly mitigate its thermal impacts, especially during daylight hours (Akram et al., 2022; Anees et al., 2024c; Pan et al., 2023). Including vegetation in urban environments can result in lowering surface temperatures of urban areas to become comparable with nearby rural areas (Aslam et al., 2022; Bhanage et al., 2023; Octarino, 2023).

The impact of different local climate zones (Stewart and Oke, 2012) on AUHI and SUHII is also vital, as variations in building density, height, and land cover type can significantly affect the intensity of both SUHII. For example, the compact high-rise buildings in Beijing contribute more to the SUHII compared to areas with scattered trees (Zheng et al., 2024). Such studies in urban areas of developed countries have provided valuable Insights into the relationship between urban morphology and SUHII. However, similar comprehensive analyses are lacking in many developing nations, particularly South Asia. With its unique combination of rapidly urbanizing cities, diverse climatic zones, and often unplanned urban expansion, Pakistan presents a distinct case for understanding SUHI dynamics. Unlike cities in developed regions, where green infrastructure is more integrated into urban planning, many Pakistani cities lack such measures, intensifying the warming effects of urbanization. Furthermore, the region's varied topography, from the mountainous northern regions to the arid plains in the south, adds complexity to the SUHII, making it distinct from regions previously studied. The current archive of scholarly literature demonstrates a significant lack of research investigating the spatial and temporal effects of SUHI in Pakistan. This gap highlights the necessity of conducting thorough research in this region to understand better the dynamics and implications of SUHI across Pakistan's growing and densifying cities, where the warming effect from removing urban vegetation remains unquantified. Addressing this important gap in the literature, our objectives were threefold: firstly, to analyze the SUHII across six Pakistani cities; secondly, to investigate the temporal trajectories of SUHII from 2010 to 2022; and thirdly, to elucidate the interrelations between SUHII and vegetation dynamics.

2. Data and methods

2.1. Study area

This study focuses on six major urban centers in Pakistan, specifically Abbottabad, Muzaffarabad, Islamabad, Peshawar, Lahore, and Sargodha (Fig. 1). The purposeful choice of these cities aims to provide a wide range of urban development stages, climate conditions, and altitudinal variations. This selection offers a thorough portrayal of the urban dynamics throughout the country (Ahmad, 2007; Qureshi and Ali, 2011). The region under consideration covers the geographical area between 33.68° and 34.35°N in latitude and 71.57° and 74.34°E in longitude. Additionally, it encompasses an elevation gradient ranging from 193 m above sea level in the plains of Sargodha to 1241 m above sea level in the hilly terrain of Abbottabad (Mohiuddin, 2007), which results in a range of regional climates (Table 1). The six cities differ in their land area covered and population growth between 2010 and 2022. These characteristics provide a unique setting for investigating the SUHII in the context of rapid urbanization. These cities collectively offer diverse opportunities for studying urban climatology due to their varying topographies (Sher et al., 2017) and varying degrees of vegetation (Chen et al., 2022; Usoltsev et al., 2020; Usoltsev et al., 2022), which can influence their local climates and urban thermal behavior.

The cities are characterized by unique differences in vegetation cover and urban infrastructure (Hayes et al., 2022; Hu et al., 2024; Liang et al., 2024), which offer valuable insights into the complex relationship between urbanization, vegetation, and local temperature trends (Andreevich et al., 2020; Anees et al., 2022b; Paschalis et al., 2021; Shahzad et al., 2024; Shobairi et al., 2022). The urban environment of

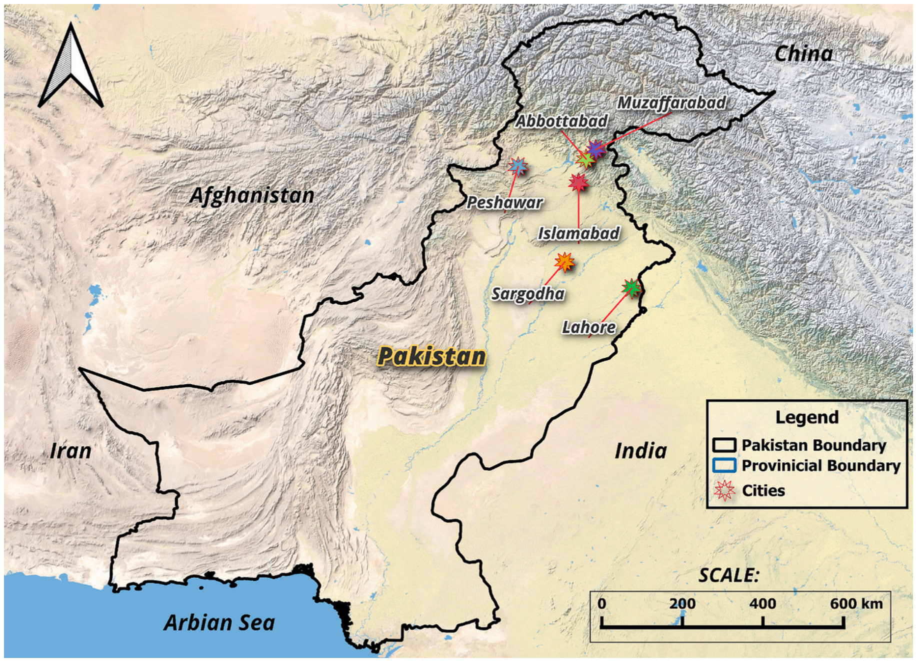

Fig. 1. Geographical map highlighting the urban centers in Pakistan investigated in this study. All six cities are of regional importance and have different climates and elevations, ranging from lowland to mountainous regions in the foothills of the Himalayan Range.

Table 1
Climatic and geographical characteristics of selected Pakistani urban centers.

Sr.No.	Cities	Lon	Lat	Mean Annual Temperature	Precipitation per year	Elevation[1]
1	Abbottabad	73.22	34.16	15.9 °C	1532 mm	1241 m
2	Muzaffarabad	73.46	34.35	12.6 °C	1308 mm	739 m
3	Islamabad	73.04	33.68	20.3 °C	1012 mm	579 m
4	Peshawar	71.57	34.00	22.3 °C	817 mm	340 m
5	Lahore	74.34	31.52	24.0 °C	636 mm	216 m
6	Sargodha	72.71	32.06	33.6 °C	440 mm	193 m

Ramirez, 2016; U.S. Geological Survey, 2017[1].

Islamabad provides a substantial quantity of green spaces, which presents a noteworthy opportunity for investigating the cooling effects of urban green infrastructure. Conversely, the urban environment of Lahore is distinguished by a significant concentration of inhabitants and a scarcity of green infrastructure, thereby exemplifying the challenges associated with addressing heat stress in swiftly expanding metropolitan areas.

2.2. Data

2.2.1. Remote sensing data acquisition and analysis

The multispectral data acquired from the Landsat-5 Thematic Mapper (TM) and in combination with the Landsat-8 Operational Landsat Imager (OLI) and thermal infrared sensors (TIRS) have been systematically collected during the summer months, particularly in June, July, and August for the years 2010, 2014, 2018 and 2022. The datasets were obtained on 26 February 2023 from the official website (http://earthexplorer.usgs.gov/) of the United States Geological Survey (USGS) (Wulder et al., 2019; Zhu, 2019). A specific scene was chosen from the Landsat imagery to encompass the entire city. As mentioned earlier, the scene played a crucial role in implementing both the classification of urban and non-urban pixels and the extraction of LST. Table 2 provides a comprehensive breakdown of the specifications of the acquired satellite imagery.

It is important to note that the thermal infrared bands (Band 6 of Landsat-5 and Bands 10 and 11 of Landsat-8) originally had a coarser

Table 2
Specifications and acquisition details of Landsat Imagery.

Landsat Product	Sensors	Bands	Spatial Resolution (m)	Cloud Cover (%)	Path/Row	Date of Acquisition
	Thematic Mapper (TM)	Band 1–5 & 7			Peshawar 151/36	
			30		Abbottabad &	
Landsat-5 TM	Thermal Infrared Sensor (TIRS)	Band 6	120		Muzaffarabad	15/06/2010
			Resampled to 30-m		150/36	
	Operational Land Imager (OLI)	Band 2–7			Islamabad	
			30	< 10	150/37	
Landsat-8 OLI	Thermal Infrared Sensor (TIRS-1/2)	Band 10	100		Lahore	26/7/2014
		Band 11	100		149/38	18/6/2018
					Sargodha	18/6/2022
					150/38	

spatial resolution of 120 m and 100 m. These bands were resampled to 30 m using bilinear interpolation to match the spatial resolution of the other multispectral bands. This method ensures consistency in the analysis by accurately aligning the data layers while maintaining spatial integrity (Mehmood et al., 2024a; Mehmood et al., 2024e). Before initiating image interpretation, spectral bands were stacked, and the region of interest was extracted. Individual city images were analyzed through a supervised classification approach using the Random Forest (RF) algorithm (Anees et al., 2024a; Anees et al., 2024b; Luo et al., 2024), segregating them into two distinct categories: urban and non-urban. Urban areas were defined as those with high population density, the extent of built-up infrastructure, and the presence of impervious surfaces, while non-urban areas were characterized by lower population density and predominantly natural or agricultural land cover (Wang et al., 2024). This classification leveraged the digital number (DN) values inherent in the respective spectral bands and ancillary data such as existing land use/land cover maps and high-resolution imagery (Truong et al., 2024).

2.2.2. Land surface temperature (LST) analysis

The LST was acquired using the standard Radiative Transfer Equation (RTE) techniques, as suggested by earlier research (Jiang and Lin, 2021; Sekertekin and Bonafoni, 2020; Yu et al., 2014a). The fundamental components of the RTE algorithm consist of the NDVI, the Proportion of Vegetation (PV), and the Land Surface Emissivity (LSE). NDVI calculation utilized Eq. (1).

$$\mathrm{NDVI} = \mathrm{NIR} + \mathrm{RED}/\mathrm{NIR}\text{–}\mathrm{RED} \tag{1}$$

where NIR denoted the near-infrared band, namely band 5, and RED represented the red band, specifically band 4, in the Landsat-8 OLI. In contrast, the Landsat-5 TM designated band 4 and band 3 as the near-infrared (NIR) and red (RED) channels, respectively, with a wavelength range of 0.64–0.67 μm. It is worth noting that there is a notable consistency between the band-4 (0.85–0.88 μm) in Landsat-8 OLI and the band-4 (0.77–0.90 μm) as well as band 3 (0.63–0.69 μm) in Landsat-5 TM. This compatibility allowed for the generation of similar outputs. Following that, Eq. (2) was utilized to get the PV, which depended on the minimum and maximum values of NDVI.

$$\mathrm{PV} = \left[\left(\mathrm{NDVI} - \mathrm{NDVI}_{\min}/\mathrm{NDVI}_{\max} - \mathrm{NDVI}_{\min}\right)\right]^2 \tag{2}$$

LSE was pivotal for extracting LST. Essentially, LSE served the dual purpose of quantifying and preserving the radiance inherent to a black body, as delineated by Planck's Law, to prognosticate the emitted radiance (Avdan and Jovanovska, 2016; Ren et al., 2022). Eq. (3), was utilized to compute the LSE:

$$LSE_{Bi} = \varepsilon_s(1 - PV) + \varepsilon_v{}^*PV + C \tag{3}$$

ε_v and ε_s denote the emissivity of vegetation and soil. Subscript *Bi* denotes the band number, and C, representing surface roughness, was set at 0.005, which is a standard approximation for smooth surfaces used in the model. While urban surfaces are generally rough due to buildings and other structures, this value helps standardize emissivity calculations in the RTE method. For bands 10 and 11, *Es* and *Ev* were 0.971 and 0.987, and 0.977 and 0.989, respectively (Sobrino and Jiménez-Muñoz, 2014). Brightness temperature from the thermal band was determined using a suitable algorithm from Landsat TM and OLI data (Anees et al., 2024a). This process involved converting the Digital Number (DN) value to radiance, as defined by NASA in Eq. (4) (US Geological Survey, 2019; USGS, 2022).

$$\mathrm{Li} = \mathrm{RADIANCEMULT}_{\mathrm{Bi}} \times \mathrm{DN} + \mathrm{RADIANCEADD}_{\mathrm{Bi}} \tag{4}$$

where *Li* denoted the sensor's spectral radiance (m W $\mathrm{cm}^{-2}\ \mathrm{sr}^{-1}\ \mu\mathrm{m}^{-1}$), quantified, whereas *RADIANCEMULT* and *RADIANCEADD* represented the respective band constants, as sourced from the accompanying header file. The brightness temperature was derived using Eq. (5) according to U.S. Geological Survey (2019):

$$Ts_{Bi} = \frac{K2_{Bi}}{log\left(\left(\frac{K1_{Bi}}{Li}\right) + 1\right)} - 273.15 \tag{5}$$

where Ts denotes the Top of Atmosphere (TOA) brightness temperature for band *i* in Kelvin, with *K1* and *K2* as constants. This method, established by the USGS, calculates the TOA brightness temperature. To convert from TOA brightness temperature to LST, atmospheric corrections were applied using the RTE, which adjusts for atmospheric influences on the spectral radiance (Hadjimitsis and Clayton, 2009). Finally, to convert LST from Kelvin to Celsius, 273.15 was subtracted from our findings (Abdullah and Barua, 2022). We employed the RTE recommended by Yu et al. (2014a), as shown in Eq. (6).

$$\mathrm{LST}_{\mathrm{RTEBi}} = \tau\ \mathrm{EiTi} + \tau\ ((1 - \mathrm{Ei})\ \mathrm{Downwelling}\ ) + \mathrm{Upwelling} \tag{6}$$

Within this framework, the symbol E represented the surface emissivity about band i, Ti signified the spectral radiance, and downwelling and upwelling refer to the path of radiance. Estimating upwelling and downwelling radiance was achieved by utilizing the MODTRAN 5.0 radiative transfer code (Coll et al., 2012; Yu et al., 2014b), with atmospheric profiles sourced from the NCEP reanalysis dataset. These profiles provide essential atmospheric parameters such as temperature, humidity, and pressure, which are necessary inputs for accurate radiative transfer simulations. The NCEP data were selected based on the closest temporal (every 6 h) and spatial ($1^\circ \times 1^\circ$ grid) proximity to the satellite overpass times and study area locations, ensuring that the atmospheric conditions modeled in MODTRAN closely represent the actual conditions during data acquisition. The ground radiance Ti was determined using Planck's law:

$$T_i = \frac{C_1}{Wavelength_{Bi}^5\left(exp\left(\frac{C_1}{Wavelength_{Bi}}Ts\right) - 1\right)} \tag{7}$$

C_1 and C_2 were Planck's radiation constants, with C_1 as $1.19104 \times 10^8\ W\,\mu m^4 m^{-2}\ sr^{-1}$ and C_2 as 14,387.7 μm *K*. 'Wavelength' denoted the bands' specific wavelengths: band 10 is 10.602 and 11 is 12.511. Surface temperature, *Ts*, was derived from Eq. (5). The RTE approach was applied to bands 10 and 11. Eq. (6) results were input into Eq. (7) to deduce the mean LST. We employed thermal band 6 of Landsat-5 and band 10 of Landsat-8 OLI for more reliable LST estimations. Band 11 was omitted due to LST estimation errors, influenced by water vapor absorption, as highlighted in prior studies (F. Wang et al., 2015).

2.3. Analysis of urban Heat Island

Researchers frequently prioritize using **LST** instead of air temperature when investigating SUHII phenomena. This preference stems from LST's superior capacity to identify surface temperature fluctuations across different areas, enhancing precision in determining SUHII intensities. This choice was supported by research conducted by Ngie et al. (2014), which emphasized the effectiveness of satellite-derived LST in offering a detailed assessment of surface temperature variations at the pixel level. Unlike air temperature, which is used to measure the traditional SUHII, LST measures surface temperature, showing much larger spatial variation, particularly during the day. The SUHII refers specifically to the difference in surface temperature between urban areas and their surrounding rural areas.

In this study, we adopted a standardized buffer with a radius of 5 km around urban areas, following the approach of Chakraborty et al. (2021), Peng et al. (2012a, 2012b), and Zhou et al. (2015). Temperature measurements for both urban and rural areas were obtained using Landsat-derived LST, as described by Eq. (8) in the work of Martin-Vide et al. (2015).

The equation was denoted as:

$$\Delta Tu - r = Tu - Tr \tag{8}$$

where $\Delta\ Tu - r$ signified the SUHII, Tu represented the urban temperature, and Tr denoted the rural temperature.

2.3.1. Statistical analysis of vegetation indicators on SUHII

A comprehensive statistical analysis was conducted to investigate the impact of FVC and the NDVI on the SUHII using Pearson's correlation analysis and linear regression (Eq. (9)) (Macarof and Statescu, 2017). The following equation represents the model:

$$Y = \beta 0 + \beta 1X + \epsilon \tag{9}$$

where Y was the dependent variable, $\beta 0$ was the y-intercept, and $\beta 1$ was the coefficient of the independent variables Xn. ϵ is the error term (the difference between the observed and predicted values). The fit and explanatory power of the model was assessed using the Residual Mean Standard Error (RMSE) and the coefficient of determination (R^2). All statistical analyses were done using R (Team, R.C, 2020). It is important to note that the SUHI, by definition, involves temperature differences between urban and rural areas. Therefore, the correlations between FVC, NDVI, and LST were calculated across the entire study area, including urban and rural environments. This ensures that the full extent of the SUHII is captured and analyzed. A trend analysis was undertaken to investigate the historical progression of SUHII in the six cities. The study period spanned from 2010 to 2022, capturing data points (locations) in 2010, 2014, 2018, and 2022.

The determination of the sites was based on specific criteria, including urban area size (measured as the total land area in square kilometers), the complexity of urban structure (quantified by the mix of residential, commercial, and industrial zones), and the diversity of land use patterns (such as the proportion of green spaces, built-up areas, and water bodies). Additionally, we ensured that each city's sample represented its overall urban environment, with sufficient statistical power to detect variations in SUHII (Athukorala and Murayama, 2020; Guo et al., 2020; D. Li et al., 2019). A linear trend analysis was utilized to examine past trends of SUHII in the chosen cities (Eq. (10)). The process entailed calculating the slope of the SUHII values across the designated period, which functions as a metric for quantifying the speed of change in SUHII. To assess the statistical significance of the observed changes in SUHII, we employed the One Sample t-test. The statistical significance of these patterns was determined using p-values ($p < 0.05$).

$$Yt = \alpha + \beta t + \epsilon t \tag{10}$$

where Yt is the dependent variable (SUHI) at time t, α is the intercept, β is the slope of the trend line indicating the rate of change in the SUHII over time, and t is the time variable (years). ϵt is the error term at time t.

2.4. Thermal hot-spot detection in urban areas

This study employed hot-spot analysis to identify urban regions with significant diurnal LST variations, focusing on areas with notable thermal anomalies. The **Getis-Ord Gi*** statistic (Getis and Ord, 1992, 2010; Ord and Getis, 1995) was used to detect spatial clusters of high (hot spots) and low (cool spots) LST values. The method calculates the local aggregation of LST values relative to neighboring features, helping to identify statistically significant thermal clusters using:

$$G_I^* = \frac{\sum_{j=1}^{n} W_{i,j}X_j - \overline{X}\sum_{j-1}^{n} W_{i,j}}{s\sqrt{\frac{\left[n\sum_{j=1}^{n} W_{i,j}^2 - \left(\sum_{j=1}^{n} W_{i,j}\right)^2\right]}{n-1}}} \tag{11}$$

wherein x_j delineates the attribute value associated with feature j: $w_{i,\ j}$ represents the spatial weight between features i and j, typically derived from their spatial relationship, and n is the aggregate count of features.

Furthermore, the mean X and variance S of the attribute values are defined as:

$$\overline{X} = \frac{\sum_{j=1}^{n} W_{i,j}}{n} \tag{12}$$

$$S = \sqrt{\frac{\sum_{J=1}^{N} X_j^2}{n} - (\overline{x})^2} \tag{13}$$

The fundamental characteristic of the Gi* statistic is its ability to calculate the local aggregation of attribute values for a specific feature compared to its neighboring features, hence contrasting it with the collection across all features (Hazaymeh et al., 2022). The presence of a statistically significant cluster is indicated by a notable departure from the expected local sum that exceeds the thresholds of random chance. This mathematical framework allowed for a systematic and comprehensive investigation of geographical patterns across urban landscapes (Chu et al., 2024; Steigerwald et al., 2022; Tsai et al., 2024; Zhao et al., 2024).

The Getis-Ord Gi* provides two main metrics: the z-score, indicating the level of clustering, and the p-value, assessing statistical significance (Ryan, 2022). High z-scores with low p-values indicate hot spots, while low z-scores with low p-values point to cool spots. Larger absolute z-scores indicate stronger clustering (Harris et al., 2017).

1. Cool-spot: Denotes regions with a significant clustering of lower LST values, characterized by a Gi^* z-score less than -1.65.
2. Hot-spot: Represents areas showcasing a significant aggregation of elevated LST values, marked by a Gi^* z-score greater than 1.65.
3. Neutral Areas: These regions do not exhibit any significant spatial correlation, falling within the z-score range of -1.65 to 1.65.

Confidence levels of 90 %, 95 %, and 99 % were applied to ensure statistical robustness. Regions were classified like "Superior Cool Zone (Tier-3)" and "Basic Hot Zone (Tier-1)" (Guerri et al., 2021; Steigerwald et al., 2022). The categories encompass a spectrum starting with "Superior Cool Zone (Tier-3)" which signifies the utmost level of confidence in cool areas and extending to "Basic Hot Zone (Tier-1)" which denotes the fundamental level of trust in hot regions. This classification scheme offers a comprehensive comprehension of the thermal dynamics exhibited by the cities Table 3.

Regions with pronounced Gi^* z-scores (either exceeding 2.58 or below -2.58) and minimal Gi^* p-values (< 0.01) are classified as Tier-3, signifying areas with extreme thermal values at a 99 % confidence level. The Inverse Distance Weighted (IDW) interpolation on the Getis-Ord Gi* results generated raster maps of hot and cool spots aligned with Landsat 5 and 8 resolutions (Yigzaw et al., 2023). These were subsequently vectorized to produce polygonal representations of the thermal

Table 3
Getis-Ord Gi* Statistic-based classification of urban thermal zones with corresponding confidence and significance Levels.

Thermal Zone Categories	Confidence Threshold	Probability (p-Value)	Standard Deviation Range (z-Score)
Superior Cool Zone (Tier-3)	99 %	<0.01	< -2.58
Intermediate Cool Zone (Tier-2)	95 %	<0.05	< -1.96
Basic Cool Zone (Tier-1)	90 %	<0.10	< -1.65
Neutral Thermal Regions	Not significant	N/A	$-1.65 <$ z-score $<$ 1.65
Basic Hot Zone (Tier-1)	90 %	<0.10	> 1.65
Intermediate Hot Zone (Tier-2)	95 %	<0.05	> 1.96
Superior Hot Zone (Tier-3)	99 %	<0.01	> 2.58

anomalies. After the Getis-Ord Gi* statistic had been employed to identify and classify thermal hot spots and cool spots, the last analytical step quantified the characteristics of vegetated areas in each of the seven thermal zones.

2.5. Vegetation and hotspot analysis in urban areas

In this research phase, information regarding the FVC and NDVI was gathered for six prominent urban areas in Pakistan. The NDVI is a universally accepted index (Mehmood et al., 2024c) that facilitates the generation of diverse vegetation maps, whereas the FVC denotes the ratio of aerial vegetation cover to ground cover (Anees et al., 2022a; Anees et al., 2024b; El-Shirbeny et al., 2022). The data were classified according to particular ranges of values:

- NDVI and FVC values less than 0.2 and 30 %, respectively, were categorized as 'Low Vegetation / No Vegetation'.
- NDVI and FVC values greater than 0.2 and 30 %, respectively, were categorized as 'High Vegetation'.

Similarly, hotspot values derived from the thermal hotspot analysis were categorized based on categories shown in Table 3. The areas associated with each category were combined and transformed into square kilometers (km^2). Lastly, the proportion of the area represented by each class of NDVI and FVC concerning the hotspot category was determined.

3. Results

3.1. Spatial and thermal dynamics of SUHII in major Pakistani cities (2010–2022)

The data exhibits a noticeable and consistent increase in the SUHII across all cities throughout the study period. Notably, **Islamabad** initially displayed characteristics of a daytime **cool island** in 2010, with a negative SUHII of −1.05 °C. However, by 2022, this shifted to a positive SUHII of 1.02 °C, indicating a significant increase in surface temperatures over the twelve years. **Peshawar** also experienced a substantial rise in its average SUHII, from 0.20 °C in 2010 to 2.51 °C in 2022. Other cities, including **Lahore, Sargodha, Abbottabad,** and **Muzaffarabad,** followed similar patterns, recording average SUHII of 1.51 °C, 1.54 °C, 1.49 °C, and 1.18 °C in 2022, respectively (Fig. 2). To ensure the reliability of our findings, we carefully selected satellite images from clear-sky, consistent seasonal conditions, reducing variability introduced by atmospheric conditions or seasonal changes. Furthermore, by analyzing over multiple years (2010, 2014, 2018, and 2022), we minimized the potential sensitivity of the results to any image used. This multi-year approach strengthens our confidence in the observed trends, as it captures a complete temporal evolution of SUHII across the cities.

Note: scale bars differ among panels.

In addition to this, an assessment of urban development measured by quantifying urban pixel counts offers further insight into the research. Islamabad experienced significant urban growth, at approximately 8.07 km^2 (8967.75 pixels) annually. While this expansion coincided with the city's SUHII rate of change, measured at 0.18 °C each year, the increase

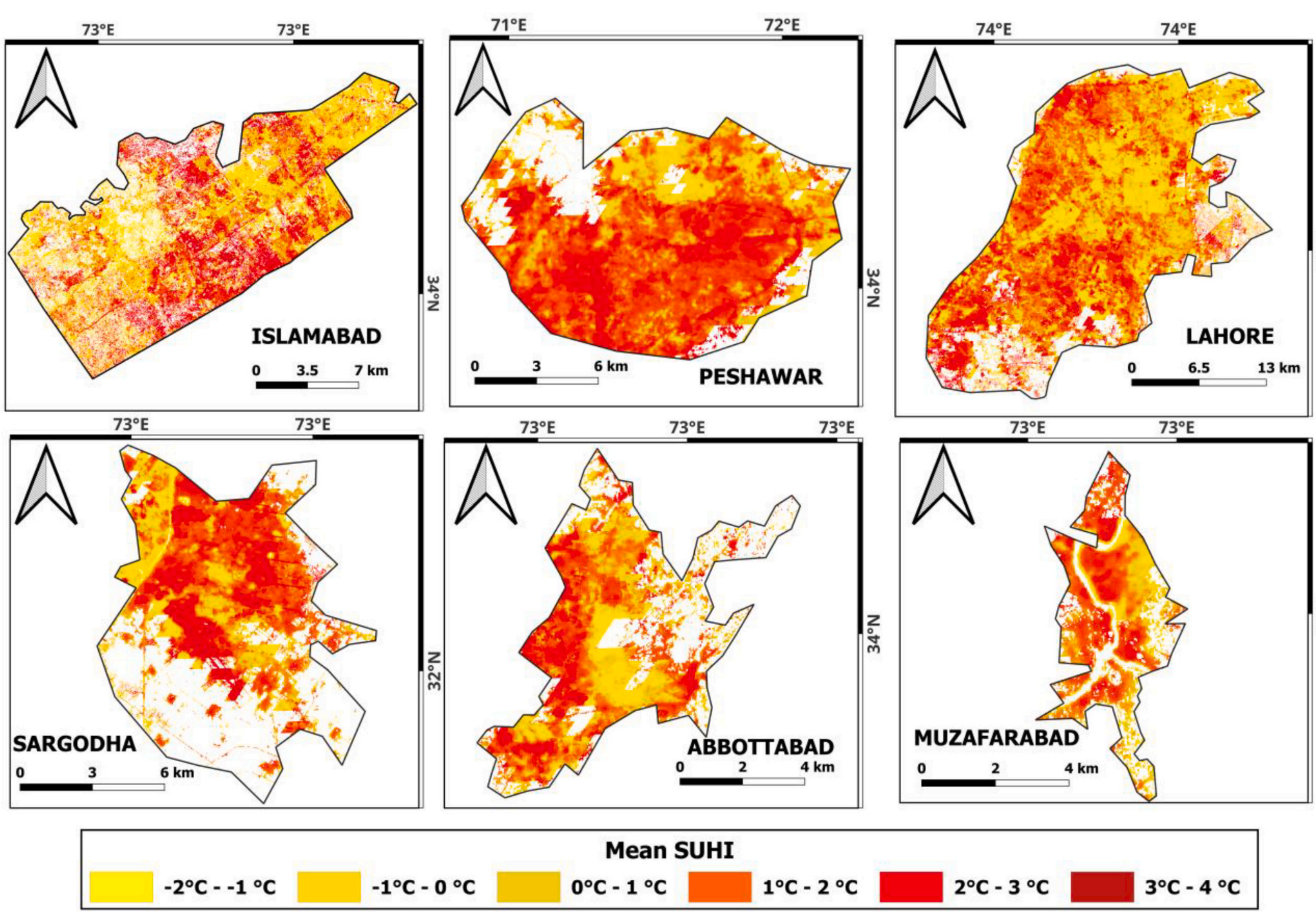

Fig. 2. Spatial distribution of mean SUHII in six major cities in Pakistan in 2022. Negative SUHII relate to cool zones where surface temperatures were below the threshold z-score defined in Table 3. Positive values indicate hot zones. White areas depict neutral thermal regions.

in SUHII may also be attributed to the intensity of urbanization, such as increased building density, surface impermeability, and reduced green spaces. These findings suggest a potential correlation between rapid urbanization and the observed rise in the SUHII. The urban growth of Peshawar exhibited a moderate pace, expanding at a rate of approximately 1.67 km^2 (1860.42 pixels) per year during the study period. However, its SUHII increased significantly by 0.19 °C per year. This suggests that factors beyond urban development alone may have contributed to the observed changes in Peshawar's SUHII. Based on our analysis, possible contributors include warming in the surrounding rural areas due to regional climate trends, changes in land cover such as reduced vegetation or altered agricultural practices, and broader climatic variability affecting both urban and rural areas. Despite experiencing a substantial annual urban expansion rate of 8.25 km^2 (9171.58 pixels), Lahore exhibited a SUHII rate of change of 0.03 °C per year, suggesting the potential effectiveness of urban heat mitigation techniques. Sargodha, Abbottabad, and Muzaffarabad displayed urban expansion rates of 0.45 km^2 (499.58 pixels), 0.65 km^2 (720.75 pixels), and 0.48 km^2 (533.83 pixels) per year, respectively (Fig. 3). These cities have also demonstrated rates of change in their SUHII of 0.03 °C per year, 0.12 °C per year, and 0.08 °C per year, respectively.

3.2. Relationship between SUHII and vegetation indices across major Pakistani cities

After analyzing six prominent cities in Pakistan, it became apparent that there exists a notable and statistically significant negative relationship between the intensity of the SUHII phenomenon and the vegetation indices, namely the NDVI and the FVC. The significance of each correlation was determined at the 0.05 level, as indicated in Table 4.

Peshawar demonstrated the highest R^2 values for NDVI and FVC, at 0.50 and 0.49, respectively. Lahore, in contrast, showed the lowest R^2 values among the studied cities, with 0.17 for NDVI and 0.12 for FVC. Sargodha and Abbottabad exhibited moderate R^2 values in their analyses. Sargodha had R^2 values of 0.39 for NDVI and 0.19 for FVC, while Abbottabad displayed R^2 values of 0.23 for NDVI and 0.20 for FVC. Both Islamabad and Muzaffarabad showed R^2 values of approximately 0.30 for both indices.

3.3. SUHII trends in six Pakistani cities: A quantitative analysis

A comprehensive trend analysis of SUHII values across six cities, Islamabad, Peshawar, Abbottabad, Sargodha, Lahore, and Muzaffarabad, revealed significant variations in urban thermal attributes. The One Sample t-test was the primary statistical method for assessing the significance of mean trends observed within these cities. Islamabad exhibits the highest average trend of 0.28, statistically significant at ($p < 0.05$), indicating a noticeable increase in SUHII values. Subsequently, Lahore (0.14), Peshawar (0.13), and Abbottabad (0.12) follow sequentially. In contrast, Muzaffarabad and Sargodha demonstrate relatively moderate average trends, with values of 0.08 and 0.06, respectively.

3.3.1. Frequency of positive and negative trends

Peshawar has had a notable presence, with 351 locations exhibiting positive trends, followed closely by Lahore, with 263 locations. Seventy-eight percent (78 %) of the sampled areas showed an upward trend. It is worth mentioning that a significant proportion of these trends, precisely 16.7 %, demonstrated statistical significance at a confidence level of 95 %. This percentage is considerably higher than the comparable rates in other cities. Islamabad and Muzaffarabad registered 182 and 198 positive trends, respectively. In contrast, Abbottabad reported 250 positive trends, which places it third in terms of the total number of positive trends observed, while Sargodha reported 89 instances. Among the cities, Peshawar had the most noteworthy trend, characterized by 75 significant trends, demonstrating an upward trend (Table 5). The distribution of Muzaffarabad displayed a total of 44 notable trends, out of which 43 were observed to be positive, with only one exception. In contrast, Sargodha exhibited a complex distribution characterized by 14 statistically significant positive and three negative trends (Fig. 4). In the

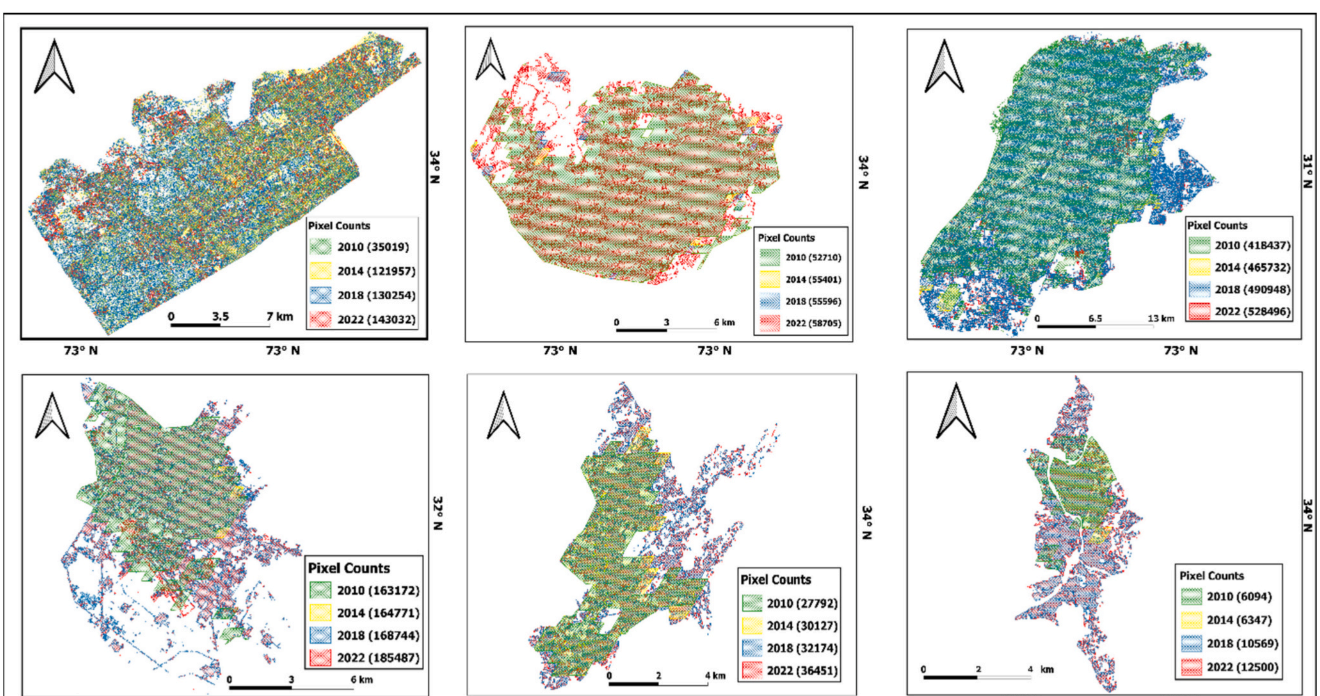

Fig. 3. Trends in urban expansion from 2010 to 2022 as measured by pixel count in six Pakistani cities. The pixel counts represent the number of pixels classified as urban based on Landsat imagery, providing insight into the spatial extent of urban growth across the six cities. These counts allow for a quantitative assessment of urban expansion and its correlation with SUHII.

Table 4
Correlation analysis between SUHII and vegetation indices in six Pakistani cities.

Cities	Vegetation cover									
	SUHII VS FVC					SUHII VS NDVI				
	R	RMSC	R^2	P-value	Sig Level	R	RMSC	R^2	p-value	Sig Level
Islamabad	−0.56	2.549	0.31	2.2e-16		−0.59	2.484	0.35	2.2e-16	
Peshawar	−0.70	1.215	0.49	2.2e-16		−0.70	1.212	0.50	2.2e-16	
Lahore	−0.36	1.423	0.12	2.032e-09		−0.42	1.385	0.17	1.432e-12	
Sargodha	−0.44	2.087	0.19	5.545e-11		−0.63	1.805	0.39	2.2e-16	
Abbottabad	−0.45	1.537	0.20	1.861e-11		−0.48	1.505	0.23	2.578e-13	
Muzaffarabad	−0.53	1.145	0.28	2.2e-16		−0.56	1.12	0.31	2.2e-16	
					0.05					0.05

Table 5
Trend analysis of SUHII across sampled locations in six Pakistani cities.

Cities	Total Sampled Locations	Mean Trend	Positive Trends	Negative Trends	Significant Trends	Significant Positive Trends	Significant Negative Trends
Islamabad	255	0.28	182	73	15	15	0
Peshawar	450	0.13	351	99	75	75	0
Lahore	380	0.14	263	117	8	8	0
Sargodha	160	0.06	89	71	17	14	3
Abbottabad	342	0.12	250	92	4	4	0
Muzaffarabad	240	0.08	198	42	44	43	1

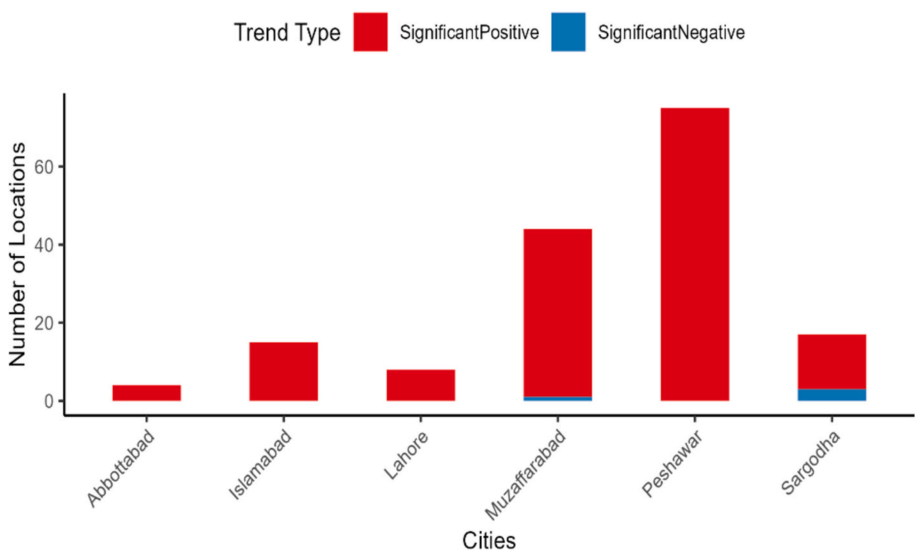

Fig. 4. Comparison of locations with significant positive (hot spots) and negative (cool spots) trend observations.

study context, it was observed that Islamabad, Lahore, and Abbottabad exhibited a consistent pattern in their significant trends, all of which displayed a positive inclination. The number of locations demonstrating these trends were recorded as 15, 8, and 4 for Islamabad, Lahore, and Abbottabad, respectively.

3.3.2. Comparative analysis

Islamabad exhibits a significant average trend, indicating that it is experiencing the most notable shift in SUHII values. Although Peshawar displays the highest number of positive trend locations, its average SUHII trend is almost half that observed in Islamabad. Nevertheless, it is worth noting that there is a substantial number of positive trends in Peshawar, which suggests a more uniform and widespread increase in the SUHII throughout the city. Muzaffarabad had a higher percentage of significant trends than the overall number of observed trends. This indicates that the changes in SUHII are less likely to be attributed to random variations. In urban areas such as Sargodha, where a relatively equal distribution of positive and negative trends exists, it becomes imperative to accurately identify major trends to distinguish actual shifts from random fluctuations. The analysis highlights the variation in SUHII changes among various urban environments. While every city has a general upward tendency, these trends' magnitude, extent, and significance differ.

3.4. Integrated analysis of vegetation and thermal hotspots in urban Pakistan

3.4.1. Thermal hotspot distribution

The thermal hotspots were classified into three distinct cool zones, namely Superior, Intermediate, Basic, and neutral thermal regions. Three hot zones were identified: Superior, Intermediate, and Basic (Fig. 5). Lahore has been identified as the city exhibiting the largest

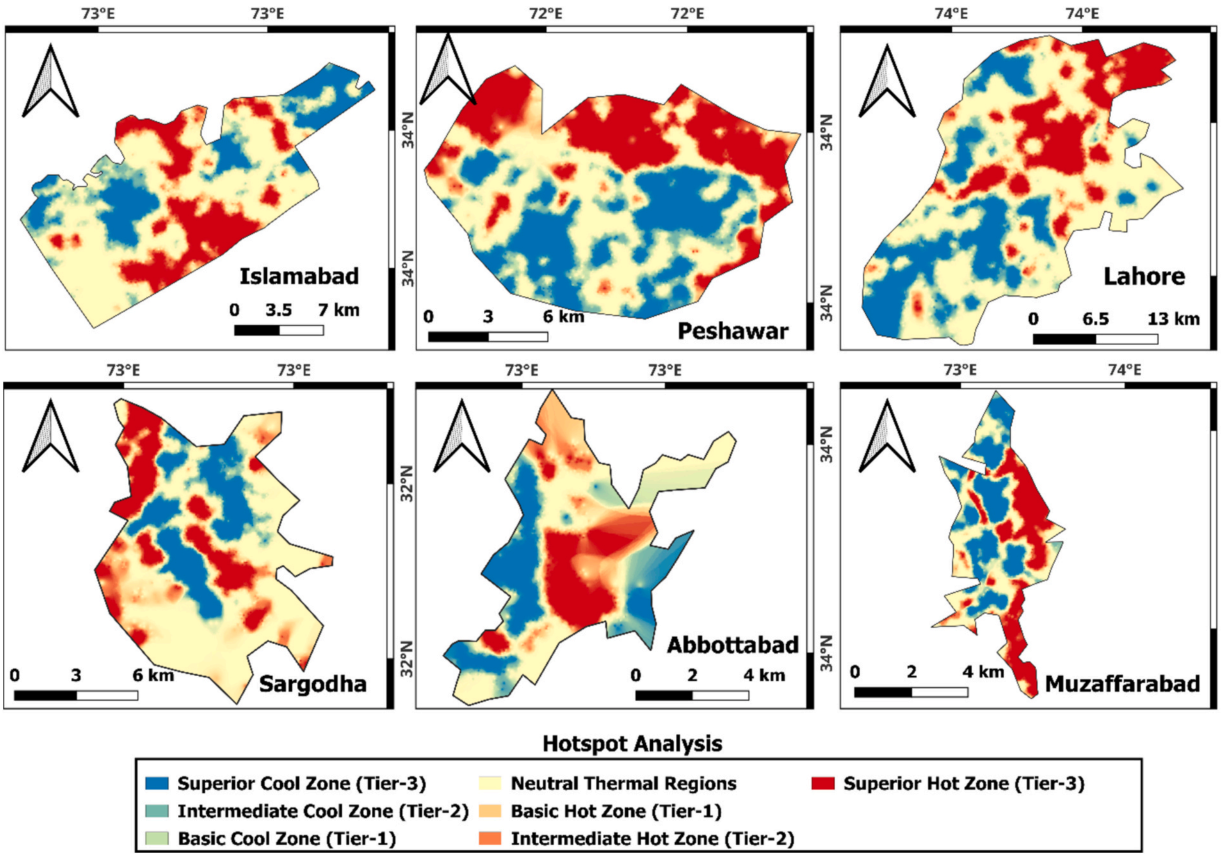

Fig. 5. Comparative analysis of hotspot categories across six Pakistani cities for the year 2022.

Superior Cool Zone, spanning an area of 111.3 km^2, and the largest Superior Hot Zone at the 90 % confidence level, covering an area of 127.1 km^2. Islamabad demonstrated a significant Neutral Thermal Region spanning an area of 103.5 km^2, which signifies the presence of regions with considerable thermal variability. The physical breadth of Superior Cool and Hot Zones differed between cities, with Muzaffarabad exhibiting the most minor distribution in both zones, measuring 12.2 km^2 and 12.1 km^2, respectively.

3.4.2. Correlation of vegetation cover with thermal hotspots

The combined NDVI and FVC data analysis with thermal hotspots yielded significant relationships. The regions classified as Superior Cool Zones exhibited a notable presence of dense vegetation, as exemplified by Islamabad (45.7 km^2) and Lahore (111.3 km^2). In contrast, the Basic and Intermediate Hot Zones had a reduced level of vegetation cover, consistent with the NDVI values indicating low or no vegetation. For example, Lahore's primary hot zone (Tier-1) covered an area of 37.9

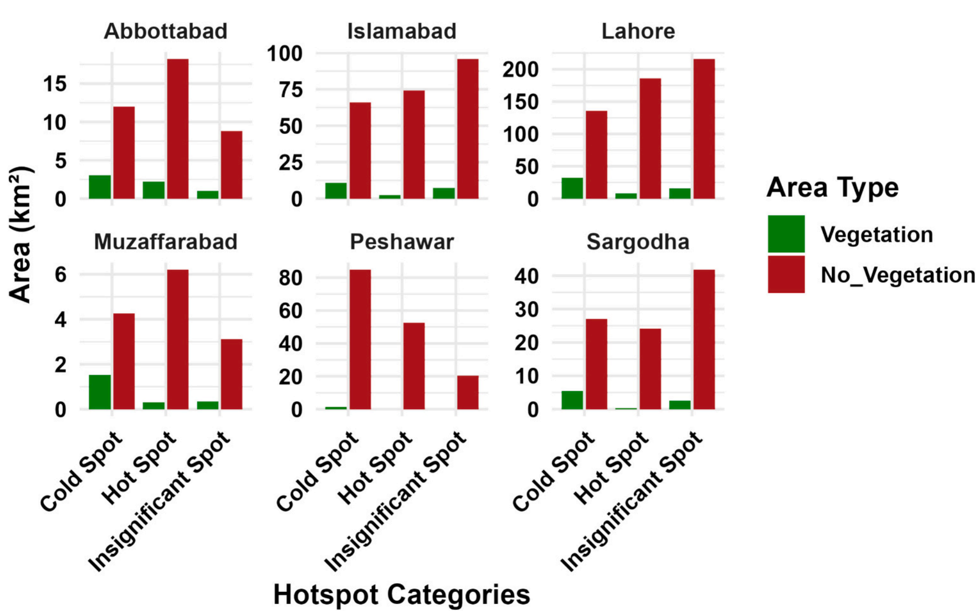

Fig. 6. Distribution of FVC areas within thermal zones across six Pakistani cities.

km^2 and was characterized by a diminished presence of vegetation (Figs. 6 and 7). Incorporating thermal hotspot data into the analysis and the NDVI and FVC indices uncovered a complex regional pattern. Metropolitan locations characterized by extensive hot zones (Badshah et al., 2024), such as Lahore and Islamabad, have also documented substantial areas devoid of vegetation, underscoring the presence of possible environmental strain and concentration of urban heat.

4. Discussion

While urbanization broadly contributes to increasing SUHII, our findings indicate that additional factors, such as the reduction of green spaces (Muhammad et al., 2023), shifts in land use patterns (e.g., from agricultural to residential areas), intensification of socioeconomic activities (e.g., transportation and commerce), and the city's unique topography and climate (Hussain et al., 2024a; Hussain et al., 2024b; Maimaitiyiming et al., 2014), play a significant role. Similar findings were reported by Yang et al. (2019), who demonstrated that natural factors, such as topography and climate, and anthropogenic influences, including population density and land use changes, play a critical role in determining LST and resulting thermal impacts. In our study, climate influences SUHII through local weather patterns, such as high solar radiation, seasonal temperature fluctuations, and humidity levels. For example, cities like Peshawar experience intense solar radiation and dry conditions, particularly in summer, intensifying surface heating. In semi-arid cities, urban-rural temperature differences are affected by time lags between radiation and water availability, with reduced rural evaporative cooling intensifying SUHII during dry seasons (Manoli et al., 2020). Similar patterns are observed in Ahmedabad, India, where rural areas exhibit higher temperatures than urban zones due to limited vegetation, creating a negative SUHII (Pir Mohammad et al., 2019). In Peshawar and surrounding regions, evapotranspiration plays a critical role in controlling surface temperatures, with improved prediction models enhancing water management in dry conditions (Gul et al., 2021). However, while irrigation can lower surface temperatures, it also raises humidity, increasing moist heat stress during extreme heat events (Mishra et al., 2020). In conclusion, heatwaves, dry spells, and reduced evapotranspiration significantly intensify the SUHII in semi-arid cities like Peshawar, where limited vegetation intensifies surface heating challenges.

In addition to urban development, topography plays a critical role in shaping SUHII in Peshawar. Recent research highlights that elevation significantly impacts heat retention and dissipation, with higher elevations experiencing cooler nighttime temperatures, while valleys trap heat, intensifying SUHI in lower regions (Haashemi et al., 2016). Peshawar, surrounded by natural barriers, is prone to heat entrapment due to its terrain, which amplifies surface temperature increases, particularly during nighttime (Mehmood et al., 2017). Temperature reversals further worsen this effect, as cooler air becomes trapped under warmer layers, increasing heat retention, especially in valley cities like Peshawar and Lahore (Khalil et al., 2022). While the topography remains fixed over the study period, regional climate changes, such as increased heatwaves and variability in precipitation, have a dynamic influence on SUHII, contributing to the intensification of surface heating. This combination of topographical features and temperature inversions contributes to the intensified SUHII observed in Peshawar. It is important to note that while urbanization and surface temperatures correlate with the SUHI effect, the concept of heat stress extends beyond surface temperatures alone. Heat stress, particularly in terms of human comfort, involves more complex measures that consider factors like air temperature, humidity, and wind conditions (Rasilla et al., 2019). While this study primarily focuses on the SUHII through surface temperature analysis, further research involving humidity data, air temperatures, and other meteorological variables would be necessary to comprehensively assess heat stress in these urban environments. This observation reinforces that SUHI is not solely driven by urbanization but is a multifaceted phenomenon influenced by both anthropogenic and natural factors (Li et al., 2020; Yang et al., 2019). This aligns with global trends identified in prior research assessing the SUHII in cities worldwide (Li et al., 2020; Wang et al., 2021).

Despite its significant spatial extent, Lahore has a comparatively modest yearly growth rate of 0.03 °C for its SUHII. This suggests that it could be possible to implement effective cooling strategies that offset continued warming from urban densification and expansion. This viewpoint is supported by a thorough examination of the relationships between urban air pollution, heat islands (Piracha and Chaudhary,

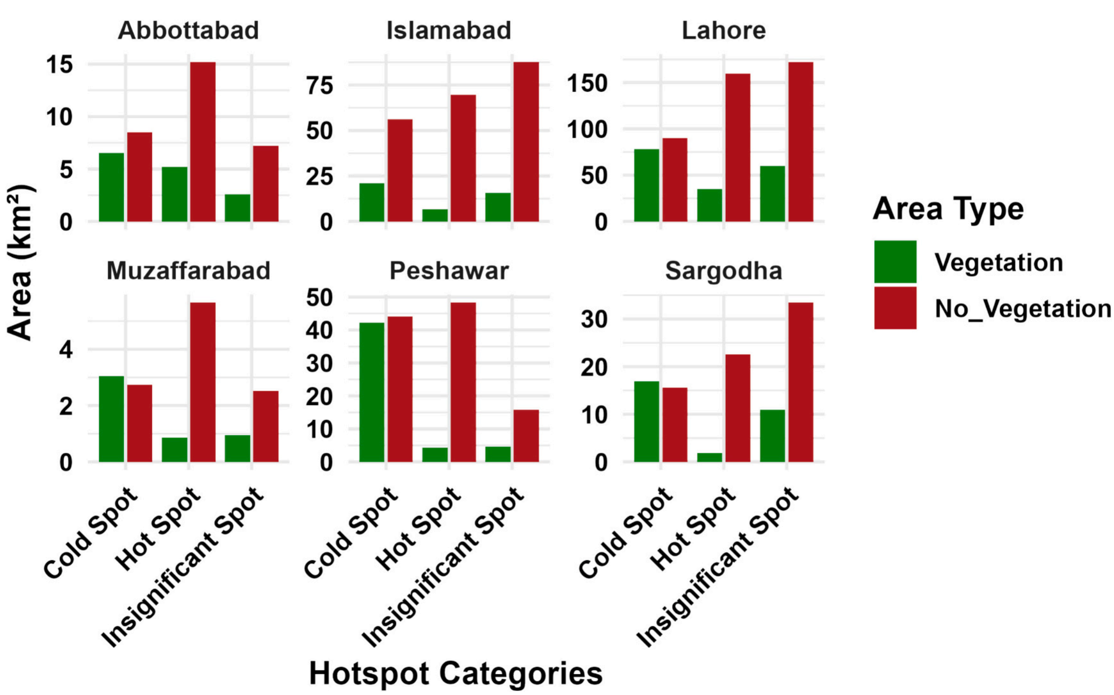

Fig. 7. Distribution of NDVI areas within thermal zones across six Pakistani cities.

2022; Rebecchi and Capolongo, 2021; Vujovic et al., 2021), and human health. The results of our study indicate varying relationships between vegetation indices and SUHII across different cities in Pakistan. In Peshawar, the high R^2 values suggest that about half of the observed variance in SUHII can be attributed to vegetation dynamics. This strong correlation underscores the significant role of vegetation in mitigating urban heat in Peshawar. Conversely, the low R^2 values in Lahore imply that while vegetation contributes to the influence of SUHII, other factors may have a more substantial impact on its urban heat island effect. This finding suggests that urban heat mitigation strategies in Lahore may need to consider a broader range of factors beyond just vegetation cover.

The moderate R^2 values observed in Sargodha and Abbottabad indicate that vegetation has a notable, though not dominant, impact on SUHII in these cities. This suggests that while urban greening initiatives could be beneficial, they should be part of a more comprehensive approach to urban heat management in these areas. The consistent R^2 values of around 0.30 for both indices in Islamabad and Muzaffarabad point to a persistent impact of vegetation on SUHII in these capital cities. This consistency across both vegetation indices reinforces the reliability of the observed relationship between vegetation and urban heat in these locations. Overall, these findings underscore vegetation's continuous cooling impact across various urban settings in Pakistan. The data consistently shows that urban areas with greater vegetation cover demonstrate a decrease in SUHII. This emphasizes the crucial role of urban greenery in moderating the adverse impacts of the urban heat island phenomenon. These results highlight the necessity of urban planning techniques that prioritize incorporating and preserving green spaces in urban designs. However, the varying strengths of correlation across cities also suggest that effective urban heat mitigation strategies may need to be tailored to the specific characteristics of each urban area, considering factors beyond just vegetation cover (Abdullah et al., 2022; Guo et al., 2022).

The urban landscape in Lahore is characterized by a thermal contradiction, as evidenced by the presence of a vast Superior Cool Zone with abundant flora and a contrasting Superior Hot Zone with limited vegetation. This spatial dichotomy highlights the importance of urban greening for moderating heat in areas with limited vegetation. Recent studies, such as those conducted during the COVID-19 lockdown (Ali et al., 2021), provide additional insights into the temporal evolution of urban heat, where reduced energy usage and emissions led to short-term changes in heat patterns. While the current study focuses on spatial thermal variations, such as the contrast between vegetated and non-vegetated regions, the temporal insights from these lockdown studies underscore the potential for targeted interventions to influence urban heat dynamics. Both spatial and temporal patterns in heat stress emphasize the importance of deliberate urban greening projects for improving the quality of urban life, as proposed by Coles and Grayson (2004) and Pancewicz et al. (2023). The methodology utilized in this study, which employs remote sensing for estimating SUHII, aligns with the approaches commended by (Bhowmick et al., 2023; Lin et al., 2022) for their efficacy in finding and examining urban heat islands. The research conducted in this study demonstrates a credible model for estimating SUHII by effectively combining remote sensing data and location-based trend analysis. This technique is particularly novel in Pakistan, as supported by the evaluations of Karunaratne et al. (2022) and Qian et al. (2023) regarding the toolbox implementation.

The methodology employed in this study involves using NDVI (Mehmood et al., 2024b; Mehmood et al., 2024d) and FVC as indicators for vegetation cover and its impact on SUHII (Li et al., 2018; Martin-Vide et al., 2015). The significant spatiotemporal variability in the urban surface thermal environment is shaped by topography, wind patterns, and anthropogenic influences, including land use changes and population density (El Kenawy et al., 2020). This complexity underscores the need for a multifaceted approach to urban planning that considers both the physical landscape and human activities to mitigate SUHII effectively.

The cities we analyzed are undergoing significant urban expansion, which mirrors the patterns observed by Radhi et al. (2015). Their findings demonstrated that urbanization processes, including construction activities and the decline of green spaces, substantially impacted air temperatures in Bahrain. Our results suggest that similar urban growth patterns could contribute to the increase in SUHII in the cities we studied, emphasizing the need for strategic urban planning to mitigate AUHI and SUHII. Including these dynamic interactions in urban climate models could lead to more accurate predictions and effective interventions. Anticipating the future, the methods and conclusions of the study establish a basis for subsequent research that incorporates longitudinal socioeconomic data (Ehrlich et al., 2021; Polinesi et al., 2020) to gain a deeper understanding of the intricate relationships among urban development, green space planning, and the SUHII. Including such factors could potentially facilitate examining the causal relationships behind these linkages, providing valuable insights for urban planners and policymakers in formulating precise actions (Li et al., 2024).

This study enhances the comprehension of urban climatology by documenting the pivotal function of vegetation in alleviating the SUHII and presenting empirical substantiation to endorse the implementation of afforestation projects. The spatial dynamics of heat and greenery emphasize the potential of focused urban design in climate change adaptation and sustainability efforts. This perspective aligns with the comprehensive evaluations of advancements and obstacles in urban development that aim to avoid accelerating urban overheating (Tian et al., 2023).

5. Conclusion

This study offers valuable insights into the spatial patterns and temporal changes of SUHII in major Pakistani cities, primarily focusing on the relationship between urban expansion, vegetation loss, and heat intensification. The results reveal a consistent upward trend in surface heat due to rapid urbanization and the decline of green spaces. Notably, cities like Islamabad, where green infrastructure has been better preserved, demonstrate lower SUHII, emphasizing the critical role of urban planning in mitigating urban heat. While advanced remote sensing techniques provide a reliable framework for assessing SUHII, particularly by using vegetation indices such as NDVI and FVC, we acknowledge that this study does not encompass the full range of factors influencing urban heat, such as air temperature or detailed ground-based measurements commonly included in broader urban climate studies. The varied success of different cities in mitigating heat further suggests that SUHI mitigation strategies should be customized to local conditions. However, the explanatory power of our analysis remains limited by its focus on surface temperature patterns and its exclusion of other significant variables like energy consumption, population density, and land use policies, which also contribute to urban heat dynamics. We also recognize that while our analysis accounted for some geographic factors, such as urban expansion and vegetation cover, it did not explicitly control elevation differences, regional climate variations, or the presence of water bodies, which could have influenced local temperature variability. Future research should aim to integrate higher-resolution data and incorporate a broader range of controlling variables, including socio-economic and environmental factors. Additionally, combining remote sensing with numerical models and ground-based observations would provide a more comprehensive understanding of the dynamics in both surface and air temperature variations in urban climates. The methods used in this study, particularly the combined use of spatial autocorrelation analysis (Getis-Ord Gi*) and vegetation indices, contribute to developing a valuable analytical framework for assessing SUHII in a developing country context. This framework could inform urban planning strategies to enhance green infrastructure to mitigate urban overheating, although further research is needed to extend these findings to broader urban climate dynamics.

Funding

This research was funded by Universiti Putra Malaysia, Malaysia, Vote No. 9750500.

Ethics approval

Not Applicable.

Consent to participate

Not Applicable.

Consent for publication

Not Applicable.

CRediT authorship contribution statement

Shoaib Ahmad Anees: Writing – review & editing, Writing – original draft, Visualization, Validation, Supervision, Software, Methodology, Investigation, Formal analysis, Data curation, Conceptualization. **Kaleem Mehmood:** Writing – review & editing, Writing – original draft, Visualization, Validation, Software, Methodology, Investigation, Formal analysis, Data curation, Conceptualization. **Syed Imran Haider Raza:** Writing – review & editing. **Sebastian Pfautsch:** Writing – review & editing. **Munawar Shah:** Writing – review & editing. **Punyawi Jamjareegulgarn:** Writing – review & editing. **Fahad Shahzad:** Writing – review & editing. **Abdullah A. Alarfaj:** Writing – review & editing. **Sulaiman Ali Alharbi:** Writing – review & editing. **Waseem Razzaq Khan:** Writing – review & editing, Investigation, Formal analysis. **Timothy Dube:** Writing – review & editing.

Declaration of competing interest

The authors declare no conflict of interest.

Data availability

https://github.com/kmkamilkhel/Ecological-Informatics

Acknowledgements

We are grateful to the Department of Forestry, The University of Agriculture, Dera Ismail Khan, 29050, Pakistan, for providing assistance and platforms for this research. We are also grateful to the Key Laboratory for Silviculture and Conservation of Ministry of Education, Beijing Forestry University, Beijing, (100083), P. R. China, for providing assistance and platforms for this research. The authors extend their appreciation to the Researchers Supporting Project number (RSP2025R98), King Saud University, Riyadh, Saudi Arabia, for financial support. Authors also acknowledge the support of the Universiti Putra Malaysia.

References

Abdullah, S., Barua, D., 2022. Modeling land surface temperature with a mono-window algorithm to estimate urban heat island intensity in an expanding urban area. Environ. Process. 9 (1), 14. https://doi.org/10.1007/s40710-021-00554-8.

Abdullah, S., Adnan, M.S.G., Barua, D., Murshed, M.M., Kabir, Z., Chowdhury, M.B.H., Hassan, Q.K., Dewan, A., 2022. Urban green and blue space changes: a spatiotemporal evaluation of impacts on ecosystem service value in Bangladesh. Eco. Inform. 70, 101730. https://doi.org/10.1016/j.ecoinf.2022.101730.

Ahmad, S., 2007. Land and water resources of Pakistan—a critical assessment. Pak. Dev. Rev. 911–937.

Akram, M., Hayat, U., Shi, J., Anees, S.A., 2022. Association of the Female Flight Ability of Asian spongy moths (*Lymantria dispar* asiatica) with locality, age and mating: a case study from China. Forests 13 (8), 1158. https://doi.org/10.3390/f13081158.

Ali, A., Ahmed, M., Hassan, N., 2021. Socioeconomic impact of COVID-19 pandemic: evidence from rural mountain community in Pakistan. J. Public Aff. 21 (4), e2355. https://doi.org/10.1002/pa.2355.

Allam, S., 2021. Green footprint calibration to addressing urban health while enhancing outdoor thermal comfort. https://doi.org/10.13189/cea.2021.090315.

Andreevich, U.V., Reza, S.S.O., Stepanovich, T.I., Amirhossein, A., Meng, Z., Anees, S.A., Petrovich, C.V., 2020. Are there differences in the response of natural stand and plantation biomass to changes in temperature and precipitation? A case for two-needled pines in Eurasia. J. Resources Ecol. 11 (4), 331. https://doi.org/10.5814/j.issn.1674-764x.2020.04.001.

Anees, S.A., Zhang, X., Khan, K.A., Abbas, M., Ghramh, H.A., Ahmad, Z., 2022a. Estimation of fractional vegetation cover dynamics and its drivers based on multi-sensor data in Dera Ismail Khan, Pakistan. J. King Saud Univ. Sci. 34 (6), 102217. https://doi.org/10.1016/j.jksus.2022.102217.

Anees, S.A., Zhang, X., Shakeel, M., Al-Kahtani, M.A., Khan, K.A., Akram, M., Ghramh, H. A., 2022b. Estimation of fractional vegetation cover dynamics based on satellite remote sensing in Pakistan: a comprehensive study on the FVC and its drivers. J. King Saud Univ. Sci. 34 (3), 101848. https://doi.org/10.1016/j.jksus.2022.101848.

Anees, S.A., Mehmood, K., Khan, W.R., Sajjad, M., Alahmadi, T.A., Alharbi, S.A., Luo, M., 2024a. Integration of machine learning and remote sensing for above ground biomass estimation through Landsat-9 and field data in temperate forests of the Himalayan region. Eco. Inform., 102732 https://doi.org/10.1016/j.ecoinf.2024.102732.

Anees, S.A., Mehmood, K., Rehman, A., Rehman, N.U., Muhammad, S., Shahzad, F., Hussain, K., Luo, M., Alarfaj, A.A., Alharbi, S.A., Khan, W.R., 2024b. Unveiling fractional vegetation cover dynamics: a spatiotemporal analysis using MODIS NDVI and machine learning. Environ. Sustain. Indicat., 100485 https://doi.org/10.1016/j.indic.2024.100485.

Anees, S.A., Yang, X., Mehmood, K., 2024c. The stoichiometric characteristics and the relationship with hydraulic and morphological traits of the Faxon fir in the subalpine coniferous forest of Southwest China. Ecol. Indic. 159, 111636. https://doi.org/10.1016/j.ecolind.2024.111636.

Aslam, B., Maqsoom, A., Khalid, N., Ullah, F., Sepasgozar, S., 2021. Urban overheating assessment through prediction of surface temperatures: a case study of Karachi, Pakistan. ISPRS Int. J. Geo Inf. 10 (8), 539. https://doi.org/10.3390/ijgi10080539.

Aslam, M.S., Huanxue, P., Sohail, S., Majeed, M.T., Rahman, S.U., Anees, S.A., 2022. Assessment of major food crops production-based environmental efficiency in China, India, and Pakistan. Environ. Sci. Pollut. Res. 1–10. https://doi.org/10.1007/s11356-021-16161-x.

Athukorala, D., Murayama, Y., 2020. Spatial variation of land use/cover composition and impact on surface urban heat island in a tropical sub-Saharan city of Accra, Ghana. Sustainability 12 (19), 7953. https://doi.org/10.3390/SU12197953.

Avdan, U., Jovanovska, G., 2016. Algorithm for automated mapping of land surface temperature using LANDSAT 8 satellite data. J. Sens. 2016 (1), 1480307. https://doi.org/10.1155/2016/1480307.

Badshah, M.T., Hussain, K., Rehman, A.U., Mehmood, K., Muhammad, B., Wiarta, R., Silamon, R.F., Khan, M.A., Meng, J., 2024. The role of random forest and markov chain models in understanding metropolitan urban growth trajectory. Front. For. Glob. Change 7, 1345047.

Bhanage, V., Kulkarni, S., Sharma, R., Lee, H.S., Gedam, S., 2023. Enumerating and modelling the seasonal alterations of surface urban heat and cool island: a case study over Indian cities. Urban Sci. 7 (2), 38. https://doi.org/10.3390/urbansci7020038.

Bhowmick, D., Mukherjee, K., Dash, P., Mondal, R., 2023, April. Use of "local climate zones" for detecting urban heat island: A case study of Kolkata metropolitan area, India. In: IOP Conference Series: Earth and Environmental Science, vol. 1164, No. 1. IOP Publishing, p. 012007. https://doi.org/10.1088/1755-1315/1164/1/012007.

Bounoua, L., Zhang, P., Mostovoy, G., Thome, K., Masek, J., Imhoff, M., Shepherd, M., Quattrochi, D., Santanello, J., Silva, J., Wolfe, R., 2015. Impact of urbanization on US surface climate. Environ. Res. Lett. 10 (8), 084010. https://doi.org/10.1088/1748-9326/10/8/084010.

Chakraborty, T.C., Lee, X., Ermida, S., Zhan, W., 2021. On the land emissivity assumption and Landsat-derived surface urban heat islands: a global analysis. Remote Sens. Environ. 265, 112682. https://doi.org/10.1016/j.rse.2021.112682.

Chen, T., Sun, A., Niu, R., 2019. Effect of land cover fractions on changes in surface urban heat islands using landsat time-series images. Int. J. Environ. Res. Public Health 16 (6), 971. https://doi.org/10.3390/ijerph16060971.

Chen, S., Yang, Y., Deng, F., Zhang, Y., Liu, D., Liu, C., Gao, Z., 2022. A high-resolution monitoring approach of canopy urban heat island using a random forest model and multi-platform observations. Atmos. Meas. Tech. 15 (3), 735–756.

Chu, Z., Li, S., Li, T., Qian, H., Liu, C., Yan, Z., 2024. Numerical simulation of layout and landscape elements on the thermal environment of urban squares. Eco. Inform. 82, 102770. https://doi.org/10.1016/j.ecoinf.2024.102770.

Coles, R., Grayson, N., 2004, October. Improving the quality of life in urban regions through urban greening initiatives–EU URGE-project. In: Open Space People Space: An International Conference on Inclusive Environments.

Coll, C., Caselles, V., Valor, E., Niclòs, R., 2012. Comparison between different sources of atmospheric profiles for land surface temperature retrieval from single channel thermal infrared data. Remote Sens. Environ. 117, 199–210.

Ehrlich, D., Melchiorri, M., Capitani, C., 2021. Population trends and urbanisation in mountain ranges of the world. Land 10 (3), 255. https://doi.org/10.3390/land10030255.

El Kenawy, A.M., Hereher, M., Robaa, S.M., McCabe, M.F., Lopez-Moreno, J.I., Domínguez-Castro, F., Gaber, I.M., Al-Awadhi, T., Al-Buloshi, A., Al Nasiri, N., Al-Hatrushi, S., 2020. Nocturnal surface urban heat island over greater Cairo: spatial

morphology, temporal trends and links to land-atmosphere influences. Remote Sens. 12 (23), 3889.
El-Shirbeny, M.A., Biradar, C., Amer, K., Paul, S., 2022. Evapotranspiration and vegetation cover classifications maps based on cloud computing at the Arab countries scale. Earth Syst. Environ. 6 (4), 837–849. https://doi.org/10.1007/s41748-022-00320-2.
Flores, R., Pereira Filho, Karam, H.A., 2016. Estimation of long term low resolution surface urban heat island intensities for tropical cities using MODIS remote sensing data. Urban Clim. 17. https://doi.org/10.1016/j.uclim.2016.04.002.
Getis, A., Ord, J.K., 1992. The analysis of spatial association by use of distance statistics. Geogr. Anal. 24 (3), 189–206. https://doi.org/10.1111/j.1538-4632.1992.tb00261.x.
Getis, A., Ord, J.K., 2010. The analysis of spatial association by use of distance statistics. In: Advances in Spatial Science, 61. https://doi.org/10.1007/978-3-642-01976-0_10.
Guerri, G., Crisci, A., Messeri, A., Congedo, L., Munafò, M., Morabito, M., 2021. Thermal summer diurnal hot-spot analysis: the role of local urban features layers. Remote Sens. 13 (3). https://doi.org/10.3390/rs13030538.
Gul, S., Ren, J., Xiong, N., Fawad, M., 2021. An effective evapotranspiration estimation scheme based on statistical indicators for sustainable environments in humid and semi-arid area of Khyber Pakhtunkhwa, Pakistan. Water Supply. https://doi.org/10.2166/ws.2021.457.
Guo, A., Yang, J., Sun, W., Xiao, X., Xia Cecilia, J., Jin, C., Li, X., 2020. Impact of urban morphology and landscape characteristics on spatiotemporal heterogeneity of land surface temperature. Sustain. Cities Soc. 63. https://doi.org/10.1016/j.scs.2020.102443.
Guo, Y., Ren, Z., Dong, Y., Hu, N., Wang, C., Zhang, P., He, X., 2022. Strengthening of surface urban heat island effect driven primarily by urban size under rapid urbanization: national evidence from China. GIScі. Remote Sens. 59 (1), 2127–2143.
Haashemi, S., Weng, Q., Darvishi, A., Alavipanah, S., 2016. Seasonal variations of the surface urban Heat Island in a semi-Arid City. Remote Sens. 8, 352. https://doi.org/10.3390/rs8040352.
Hadjimitsis, D.G., Clayton, C., 2009. Determination of aerosol optical thickness through the derivation of an atmospheric correction for short-wavelength Landsat TM and ASTER image data: an application to areas located in the vicinity of airports at UK and Cyprus. Appl. Geomat. 1 (1–2). https://doi.org/10.1007/s12518-009-0004-2.
Haider, K., Khokhar, M.F., Chishtie, F., RazzaqKhan, W., Hakeem, K.R., 2017. Identification and future description of warming signatures over Pakistan with special emphasis on evolution of CO 2 levels and temperature during the first decade of the twenty-first century. Environ. Sci. Pollut. Res. 24, 7617–7629.
Haris, M., Hussain, T., Mohamed, H.I., Khan, A., Ansari, M.S., Tauseef, A., Khan, A.A., Akhtar, N., 2023. Nanotechnology – a new frontier of nano-farming in agricultural and food production and its development. In: Science of the Total Environment, 857. https://doi.org/10.1016/j.scitotenv.2022.159639.
Harris, N.L., Goldman, E., Gabris, C., Nordling, J., Minnemeyer, S., Ansari, S., Lippmann, M., Bennett, L., Raad, M., Hansen, M., Potapov, P., 2017. Using spatial statistics to identify emerging hot spots of forest loss. Environ. Res. Lett. 12 (2), 024012.
Hayes, A.T., Jandaghian, Z., Lacasse, M.A., Gaur, A., Lu, H., Laouadi, A., Ge, H., Wang, L., 2022. Nature-based solutions (NBSs) to mitigate urban Heat Island (UHI) effects in Canadian cities. Buildings 12 (7). https://doi.org/10.3390/buildings12070925.
Hazaymeh, K., Almagbile, A., Alomari, A.H., 2022. Spatiotemporal analysis of traffic accidents hotspots based on geospatial techniques. ISPRS Int. J. Geo Inf. 11 (4). https://doi.org/10.3390/ijgi11040260.
Hu, Y., Wu, Y., Tantian, Z., Sun, G., 2024. Capturing urban green view with mobile crowd sensing. Eco. Inform. 81, 102640. https://doi.org/10.1016/j.ecoinf.2024.102640.
Huang, F., Zhan, W., Wang, Z.H., Voogt, J., Hu, L., Quan, J., Liu, C., Zhang, N., Lai, J., 2020a. Satellite identification of atmospheric-surface-subsurface urban heat islands under clear sky. Remote Sens. Environ. 250. https://doi.org/10.1016/j.rse.2020.112039.
Huang, H., Deng, X., Yang, H., Li, S., Li, M., 2020b. Spatial evolution of the effects of urban heat island on residents' health. Tehnicki Vjesnik 27 (5). https://doi.org/10.17559/TV-20200503211912.
Hussain, K., Mehmood, K., Anees, S.A., Ding, Z., Muhammad, S., Badshah, T., Shahzad, F., Haidar, I., Wahab, A., Ali, J., Ansari, M.J., 2024a. Assessing Forest fragmentation due to land use changes from 1992 to 2023: a spatio-temporal analysis using remote sensing data. Heliyon. https://doi.org/10.1016/j.heliyon.2024.e34710.
Hussain, K., Mehmood, K., Yujun, S., Badshah, T., Anees, S.A., Shahzad, F., Nooruddin, Ali J., Bilal, M., 2024b. Analysing LULC transformations using remote sensing data: insights from a multilayer perceptron neural network approach. Ann. GIS 1–27. https://doi.org/10.1080/19475683.2024.2343399.
Jallat, H., Khokhar, M.F., Kudus, K.A., Nazre, M., Saqib, N.U., Tahir, U., Khan, W.R., 2021. Monitoring carbon stock and land-use change in 5000-year-old juniper forest stand of Ziarat, Balochistan, through a synergistic approach. Forests 12 (1), 51.
Jiang, Y., Lin, W.P., 2021. A comparative analysis of retrieval algorithms of land surface temperature from landsat-8 data: a case study of Shanghai, China. Int. J. Environ. Res. Public Health 18 (11). https://doi.org/10.3390/ijerph18115659.
Karunaratne, S., Athukorala, D., Murayama, Y., Morimoto, T., 2022. Assessing surface urban Heat Island related to land use/land cover composition and pattern in the Temperate Mountain Valley City of Kathmandu, Nepal. Remote Sens. 14 (16). https://doi.org/10.3390/rs14164047.
Khalil, U., Azam, U., Aslam, B., Ullah, I., Tariq, A., Li, Q., Lu, L., 2022. Developing a spatiotemporal model to forecast land surface temperature: a way forward for better town planning. Sustainability. https://doi.org/10.3390/su141911873.
Khan, W.R., Rasheed, F., Zulkifli, S.Z., Kasim, M.R.B.M., Zimmer, M., Pazi, A.M., Kamrudin, N.A., Zafar, Z., Faridah-Hanum, I., Nazre, M., 2020. Phytoextraction potential of *Rhizophora apiculata*: a case study in Matang mangrove forest reserve, Malaysia. Tropic. Conserv. Sci. 13, 1940082920947344.
Khan, W.R., Nazre, M., Akram, S., Anees, S.A., Mehmood, K., Ibrahim, F.H., Zhu, X., 2024. Assessing the productivity of the Matang mangrove forest reserve: review of one of the best-managed mangrove forests. Forests 15 (5), 747. https://doi.org/10.3390/f15050747.
Koomen, E., Diogo, V., 2017. Assessing potential future urban heat island patterns following climate scenarios, socioeconomic developments and spatial planning strategies. Mitig. Adapt. Strateg. Glob. Chang. 22 (2). https://doi.org/10.1007/s11027-015-9646-z.
Li, H., Zhou, Y., Li, X., Meng, L., Wang, X., Wu, S., Sodoudi, S., 2018. A new method to quantify surface urban heat island intensity. Sci. Total Environ. 624. https://doi.org/10.1016/j.scitotenv.2017.11.360.
Li, D., Liao, W., Rigden, A.J., Liu, X., Wang, D., Malyshev, S., Shevliakova, E., 2019. Urban heat island: aerodynamics or imperviousness? Sci. Adv. 5 (4). https://doi.org/10.1126/sciadv.aau4299.
Li, L., Zha, Y., Zhang, J., 2020. Spatially non-stationary effect of underlying driving factors on surface urban heat islands in global major cities. Int. J. Appl. Earth Obs. Geoinf. 90. https://doi.org/10.1016/j.jag.2020.102131.
Li, J., Zhao, Y., Chen, D., Zhao, P., Zhang, C., Wang, Y., 2024. The quantitative role of moisture and vertical motion in shaping summer heavy rainfall over North China under two distinct large-scale weather patterns. J. Clim. 37 (8), 2655–2672. https://doi.org/10.1175/JCLI-D-22-0850.1.
Liang, C., Jiang, H., Yang, S., Tian, P., Ma, X., Tang, Z., Wang, H., Wang, W., 2024. Characterizing street trees in three metropolises of Central China by using street view data: from individual trees to landscape mapping. Eco. Inform. 80, 102480. https://doi.org/10.1016/j.ecoinf.2024.102480.
Lin, L., Meng, L., Mei, Y., Zhang, W., Liu, H., Xiang, W., 2022. Spatial–temporal patterns of summer urban islands and their economic implications in Beijing. Environ. Sci. Pollut. Res. 29 (22). https://doi.org/10.1007/s11356-021-18029-6.
Luo, M., Anees, S.A., Huang, Q., Qin, X., Qin, Z., Fan, J., Han, G., Zhang, L., Shafri, H.Z.M., 2024. Improving Forest above-ground biomass estimation by integrating individual machine learning models. Forests 15 (6), 975. https://doi.org/10.3390/f15060975.
Macarof, P., Statescu, F., 2017. Comparasion of NDBI and NDVI as indicators of surface urban Heat Island effect in Landsat 8 imagery: a case study of Iasi. Present Environ. Sustain. Developm. 11 (2). https://doi.org/10.1515/pesd-2017-0032.
Maimaitiyiming, M., Ghulam, A., Tiyip, T., Pla, F., Latorre-Carmona, P., Halik, Ü., Sawut, M., Caetano, M., 2014. Effects of green space spatial pattern on land surface temperature: implications for sustainable urban planning and climate change adaptation. ISPRS J. Photogramm. Remote Sens. 89, 59–66.
Manoli, G., Fatichi, S., Bou-Zeid, E., Katul, G., 2020. Seasonal hysteresis of surface urban heat islands. Proc. Natl. Acad. Sci. 117, 7082–7089. https://doi.org/10.1073/pnas.1917554117.
Martin-Vide, J., Sarricolea, P., Moreno-García, M.C., 2015. On the definition of urban heat island intensity: the "rural" reference. Front. Earth Sci. 3. https://doi.org/10.3389/feart.2015.00024.
Mathew, A., Chaudhary, R., Gupta, N., 2015. Study of urban heat island effect on Ahmedabad City and its relationship with urbanization and vegetation parameters. Int. J. Comp. Math. Sci. 4 (March).
Mehmood, K., Anees, S.A., Luo, M., Akram, M., Zubair, M., Khan, K.A., Khan, W.R., 2024a. Assessing Chilgoza pine (*Pinus gerardiana*) Forest fire severity: remote sensing analysis, correlations, and predictive modeling for enhanced management strategies. Trees For. People, 100521. https://doi.org/10.1016/j.tfp.2024.100521.
Mehmood, K., Anees, S.A., Muhammad, S., Hussain, K., Shahzad, F., Liu, Q., Ansari, M.J., Alharbi, S.A., Khan, W.R., 2024b. Analyzing vegetation health dynamics across seasons and regions through NDVI and climatic variables. Sci. Rep. 14 (1), 11775. https://doi.org/10.1038/s41598-024-62464-7.
Mehmood, K., Anees, S.A., Rehman, A., Rehman, N.U., Muhammad, S., Shahzad, F., Liu, Q., Alharbi, S.A., Alfarraj, S., Ansari, M.J., Khan, W.R., 2024c. Assessment of Climatic Influences on Net Primary Productivity along Elevation Gradients in Temperate Ecoregions. Trees, Forests and People, p. 100657.
Mehmood, K., Anees, S.A., Rehman, A., Tariq, A., Liu, Q., Muhammad, S., Rabbi, F., Pan, S.A., Hatamleh, W.A., 2024d. Assessing forest cover changes and fragmentation in the Himalayan temperate region: implications for forest conservation and management. J. For. Res. 35 (1), 82. https://doi.org/10.1007/s11676-024-01734-6.
Mehmood, K., Anees, S.A., Rehman, A., Tariq, A., Zubair, M., Liu, Q., Rabbi, F., Khan, K.A., Luo, M., 2024e. Exploring spatiotemporal dynamics of NDVI and climate-driven responses in ecosystems: insights for sustainable management and climate resilience. Eco. Inform., 102532 https://doi.org/10.1016/j.ecoinf.2024.102532.
Mehmood, A., Mahmood, A., Eqani, S.A.M.A.S., Ishtiaq, M., Ashraf, A., Bibi, N., Qadir, A., Li, J., Zhang, G., 2017. A review on emerging persistent organic pollutants: Current scenario in Pakistan. Human and Ecological Risk. Assessment: An Inter. J. 23 (1), 1–13.
Mishra, V., Ambika, A., Asoka, A., Aadhar, S., Buzan, J., Kumar, R., Huber, M., 2020. Moist heat stress extremes in India enhanced by irrigation. Nat. Geosci. 13, 722–728. https://doi.org/10.1038/s41561-020-00650-8.
Mohammad, P., Goswami, A., Bonafoni, S., 2019. The impact of the land cover dynamics on surface urban Heat Island variations in semi-arid cities: a case study in Ahmedabad City, India, using multi-sensor/source data. Sensors (Basel, Switzerland) 19. https://doi.org/10.3390/s19173701.

Mohiuddin, Y.N., 2007. Pakistan: a global studies handbook. ABC-CLIO.
Monteiro, F.F., Gonçalves, W.A., de Andrade, L.M.B., Villavicencio, L.M.M., dos Santos Silva, C.M., 2021. Assessment of urban Heat Islands in Brazil based on MODIS remote sensing data. Urban Clim. 35. https://doi.org/10.1016/j.uclim.2020.100726.
Muhammad, S., Hamza, A., Mehmood, K., Adnan, M., Tayyab, M., 2023. Analyzing the impact of forest harvesting ban in northern temperate forest. A case study of Anakar Valley, Kalam swat region, Khyber-Pakhtunkhwa, Pakistan. Pure Appl. Biol. 12 (2), 1434–1439.
Ngie, A., Abutaleb, K., Ahmed, F., Darwish, A., Ahmed, M., 2014. Assessment of urban heat island using satellite remotely sensed imagery: a review. S. Afr. Geogr. J. 96 (2). https://doi.org/10.1080/03736245.2014.924864.
Octarino, C.N., 2023. Efektivitas Pertanian Perkotaan (Urban Farming) dalam Mitigasi Urban Heat Island di Kawasan Perkotaan. ATRIUM: Jurnal Arsitektur 8 (3). https://doi.org/10.21460/atrium.v8i3.200.
Ord, J.K., Getis, A., 1995. Local spatial autocorrelation statistics: distributional issues and an application. Geogr. Anal. 27 (4). https://doi.org/10.1111/j.1538-4632.1995.tb00912.x.
Pan, S.A., Anees, S.A., Li, X., Yang, X., Duan, X., Li, Z., 2023. Spatial and temporal patterns of non-structural carbohydrates in Faxon fir (Abies fargesii var. faxoniana), Subalpine Mountains of Southwest China. Forests 14 (7), 1438. https://doi.org/10.3390/f14071438.
Pancewicz, A., Bednarz, D., Drożdż, D., Marszoł, M., Suchy, N., 2023. The use of nature-based solutions in the adaptation of large polish cities to climate change and energy transformation: a comparative analysis. Energies 16 (13). https://doi.org/10.3390/en16135189.
Paschalis, A., Chakraborty, T., Fatichi, S., Meili, N., Manoli, G., 2021. Urban forests as main regulator of the evaporative cooling effect in cities. AGU Adv. 2 (2). https://doi.org/10.1029/2020av000303.
Peng, S., Piao, S., Ciais, P., Friedlingstein, P., Ottle, C., Bréon, F.M., Nan, H., Zhou, L., Myneni, R.B., 2012a. Response to comment on "Surface urban heat island across 419 global big cities.". Environ. Sci. Technol. 46 (12). https://doi.org/10.1021/es301811b.
Peng, S., Piao, S., Ciais, P., Friedlingstein, P., Ottle, C., Bréon, F.M., Nan, H., Zhou, L., Myneni, R.B., 2012b. Surface urban heat island across 419 global big cities. Environ. Sci. Technol. 46 (2). https://doi.org/10.1021/es2030438.
Piracha, A., Chaudhary, M.T., 2022. Urban air pollution, urban Heat Island and human health: a review of the literature. Sustainability (Switzerland) 14 (15). https://doi.org/10.3390/su14159234.
Pison, G., 2022. World population: 8 billion today, how many tomorrow? Popul. Societies 604. https://doi.org/10.3917/popsoc.604.0001.
Polinesi, G., Recchioni, M.C., Turco, R., Salvati, L., Rontos, K., Rodrigo-Comino, J., Benassi, F., 2020. Population trends and urbanization: Simulating density effects using a local regression approach. ISPRS Int. J. Geo Inf. 9 (7). https://doi.org/10.3390/ijgi9070454.
Qian, J., Meng, Q., Zhang, L., Schlink, U., Hu, X., Gao, J., 2023. Characteristics of anthropogenic heat with different modeling ideas and its driving effect on urban heat islands in seven typical Chinese cities. Sci. Total Environ. 886. https://doi.org/10.1016/j.scitotenv.2023.163989.
Qureshi, N.A., Ali, Z., 2011. Climate change, biodiversity Pakistan's scenario. J. Anim. Plant Sci. 21 (2 Suppl), 358–363.
Radhi, H., Sharples, S., Assem, E., 2015. Impact of urban heat islands on the thermal comfort and cooling energy demand of artificial islands - a case study of AMWAJ Islands in Bahrain. Sustain. Cities Soc. 19. https://doi.org/10.1016/j.scs.2015.07.017.
Ramirez, E., 2016. U.S. Releases Enhanced Shuttle Land Elevation Data. Nasa.
Rasilla, D., Allende, F., Martilli, A., Fernández, F., 2019. Heat waves and human well-being in Madrid (Spain). Atmosphere. https://doi.org/10.3390/ATMOS10050288.
Rebecchi, A., Capolongo, S., 2021. Healthy design and urban planning strategies framing the SDG 11 sustainable cities and communities. Eur. J. Pub. Health 31 (Supplement_3). https://doi.org/10.1093/eurpub/ckab164.733.
Ren, Z., Fu, Y., Dong, Y., Zhang, P., He, X., 2022. Rapid urbanization and climate change significantly contribute to worsening urban human thermal comfort: a national 183-city, 26-year study in China. Urban Clim. 43, 101154.
Ryan, B.J., 2022. Analyzing Climate Change and Extreme Weather Event Impacts on Human Migration and Vulnerability in the Southeastern United States (2004–2018). Master's thesis. Auburn University.
Scolio, M., Kremer, P., Zhang, Y., Shakya, K.M., 2024. Spatial-temporal modeling of the relationship between surface temperature and air temperature in metropolitan urban systems. Urban Clim. 55, 101921.
Sekertekin, A., Bonafoni, S., 2020. Land surface temperature retrieval from Landsat 5, 7, and 8 over rural areas: assessment of different retrieval algorithms and emissivity models and toolbox implementation. Remote Sens. 12 (2). https://doi.org/10.3390/rs12020294.
Shahzad, F., Mehmood, K., Hussain, K., Haidar, I., Anees, S.A., Muhammad, S., Ali, J., Adnan, M., Wang, Z., Feng, Z., 2024. Comparing machine learning algorithms to predict vegetation fire detections in Pakistan. Fire Ecol. 20 (1), 1–20. https://doi.org/10.1186/s42408-024-00289-5.
Sher, H., Barkworth, M.E., de Boer, H.J., 2017. Medicinal and aromatic plant cultivation in the swat valley, North-Western Pakistan, for economic development and biodiversity conservation. Genet. Resour. Crop. Evol. 64, 237–245.
Shobairi, S.O.R., Lin, H., Usoltsev, V.A., Osmirko, A.A., Tsepordey, I.S., Ye, Z., Anees, S.A., 2022. A comparative pattern for Populus spp. and Betula spp. stand biomass in Eurasian climate gradients. Croat. J. For. Eng. J. Theory Appl. For. Eng. 43 (2), 457–467. https://doi.org/10.5552/crojfe.2022.1340.
Sobrino, J.A., Jiménez-Muñoz, J.C., 2014. Minimum configuration of thermal infrared bands for land surface temperature and emissivity estimation in the context of potential future missions. Remote Sens. Environ. 148, 158–167.
Soltani, A., Sharifi, E., 2019. Understanding and analysing the urban heat island (UHI) effect in micro-scale. Int. J. Soc. Ecol. Sustain. Developm. 10 (2). https://doi.org/10.4018/IJSESD.2019040102.
Steigerwald, F., Kossmann, M., Schau-Noppel, H., Buchholz, S., Panferov, O., 2022. Delimitation of urban hot spots and rural cold air formation areas for nocturnal ventilation studies using urban climate simulations. Land 11 (8). https://doi.org/10.3390/land11081330.
Stewart, I.D., Oke, T.R., 2012. Local climate zones for urban temperature studies. Bull. Am. Meteorol. Soc. 93 (12), 1879–1900.
Stewart, I.D., Krayenhoff, E.S., Voogt, J.A., Lachapelle, J.A., Allen, M.A., Broadbent, A.M., 2021. Time evolution of the surface urban Heat Island. Earth's Future 9 (10). https://doi.org/10.1029/2021EF002178.
Team, R.C, 2020. RA Language and Environment for Statistical Computing. R Foundation for Statistical Computing.
Tian, D., Zhang, J., Gao, Z., 2023. The advancement of research in cool roof: super cool roof, temperature-adaptive roof and crucial issues of application in cities. Energy Build. 291. https://doi.org/10.1016/j.enbuild.2023.113131.
Truong, V.T., Hirayama, S., Phan, D.C., Hoang, T.T., Tadono, T., Nasahara, K.N., 2024. JAXA's new high-resolution land use land cover map for Vietnam using a time-feature convolutional neural network. Sci. Rep. 14 (1), 3926.
Tsai, C.W., Lin, M.-L., Tung, J.Y., 2024. Spatial and temporal evolution of heatwaves in Taiwan in a changing climate using multi-dimensional complementary ensemble empirical mode decomposition. Eco. Inform. 81, 102585. https://doi.org/10.1016/j.ecoinf.2024.102585.
U.S. Geological Survey, 2017. Shuttle Radar Topography Mission 1 Arc-Second Global. U.S. Geological Survey.
U.S. Geological Survey, 2019. Landsat 8 data users handbook. Nasa 8 (November).
USGS, 2022. Landsat 9 Data Users Handbook Version 1.0. Nasa, February.
Usoltsev, V.A., Chen, B., Shobairi, S.O.R., Tsepordey, I.S., Chasovskikh, V.P., Anees, S.A., 2020. Patterns for Populus spp. stand biomass in gradients of winter temperature and precipitation of Eurasia. Forests 11 (9), 906. https://doi.org/10.3390/f11090906.
Usoltsev, V.A., Lin, H., Shobairi, S.O.R., Tsepordey, I.S., Ye, Z., Anees, S.A., 2022. The principle of space-for-time substitution in predicting Betula spp. biomass change related to climate shifts. Appl. Ecol. Environ. Res. 20 (4), 3683–3698. https://doi.org/10.15666/aeer/2004_36833698.
Vujovic, S., Haddad, B., Karaky, H., Sebaibi, N., Boutouil, M., 2021. Urban Heat Island: causes, consequences, and mitigation measures with emphasis on reflective and permeable pavements. CivilEng 2 (2). https://doi.org/10.3390/civileng2020026.
Wang, F., Qin, Z., Song, C., Tu, L., Karnieli, A., Zhao, S., 2015. An improved mono-window algorithm for land surface temperature retrieval from landsat 8 thermal infrared sensor data. Remote Sens. 7 (4). https://doi.org/10.3390/rs70404268.
Wang, R., Gao, W., Zhou, N., Kammen, D.M., Peng, W., 2021. Urban structure and its implication of heat stress by using remote sensing and simulation tool. Sustain. Cities Soc. 65. https://doi.org/10.1016/j.scs.2020.102632.
Wang, C., Ren, Z., Du, Y., Guo, Y., Zhang, P., Wang, G., Li, T., 2023. Urban vegetation cooling capacity was enhanced under rapid urbanization in China. J. Clean. Prod. 425, 138906.
Wang, C., Ren, Z., Guo, Y., Zhang, P., Hong, S., Ma, Z., Wang, X., 2024. Assessing urban population exposure risk to extreme heat: patterns, trends, and implications for climate resilience in China (2000–2020). Sustain. Cities Soc. 103, 105260.
Wu, X., Wang, G., Yao, R., Wang, L., Yu, D., Gui, X., 2019. Investigating surface urban heat islands in South America based on MODIS data from 2003-2016. Remote Sens. 11 (10). https://doi.org/10.3390/rs11101212.
Wulder, M.A., Loveland, T.R., Roy, D.P., Crawford, C.J., Masek, J.G., Woodcock, C.E., Allen, R.G., Anderson, M.C., Belward, A.S., Cohen, W.B., Dwyer, J., Erb, A., Gao, F., Griffiths, P., Helder, D., Hermosilla, T., Hipple, J.D., Hostert, P., Hughes, M.J., Zhu, Z., 2019. Current status of Landsat program, science, and applications. Remote Sens. Environ. 225. https://doi.org/10.1016/j.rse.2019.02.015.
Xiang, Y., Zheng, B., Bedra, K.B., Ouyang, Q., Liu, J., Zheng, J., 2023. Spatial and seasonal differences between near surface air temperature and land surface temperature for urban Heat Island effect assessment. Urban Clim. 52, 101745.
Xu, H., Li, Q., Chen, J., 2022. Highlight removal from a single grayscale image using attentive GAN. Appl. Artif. Intell. 36 (1), 1988441. https://doi.org/10.1080/08839514.2021.1988441.
Yang, L., Niyogi, D., Tewari, M., Aliaga, D., Chen, F., Tian, F., Ni, G., 2016. Contrasting impacts of urban forms on the future thermal environment: example of Beijing metropolitan area. Environ. Res. Lett. 11 (3). https://doi.org/10.1088/1748-9326/11/3/034018.
Yang, Y.J., Gao, Z., Shi, T., Wang, H., Li, Y., Zhang, N., Huang, Y., 2019. Assessment of urban surface thermal environment using MODIS with a population-weighted method: a case study. J. Spat. Sci. 64 (2), 287–300.
Yigzaw, Y., Mekuriaw, A., Amsalu, T., 2023. Analyzing physical and socioeconomic factors for property crime incident in Addis Ababa, Ethiopia. Heliyon 9 (2). https://doi.org/10.1016/j.heliyon.2023.e13282.
Yu, X., Guo, X., Wu, Z., 2014a. Land surface temperature retrieval from landsat 8 TIRS-comparison between radiative transfer equation-based method, split window algorithm and single channel method. Remote Sens. 6 (10). https://doi.org/10.3390/rs6109829.
Yu, X., Guo, X., Wu, Z., 2014b. Land surface temperature retrieval from Landsat 8 TIRS—comparison between radiative transfer equation-based method, split window algorithm and single channel method. Remote Sens. 6 (10), 9829–9852.

Zhang, L., Luo, F., Pan, G., Zhang, W., Ren, G., Zheng, Z., Yang, Y., 2024a. Elucidating the multi-timescale variability of a canopy urban Heat Island by using the short-time Fourier transform. Geophys. Res. Lett. 51 (1), e2023GL106221.
Zhang, W., Dai, L., Yan, Y., Han, X., Teng, Y., Li, M., Zhu, Y., Zhang, Y., 2024b. Multiscale geographically weighted regression-based analysis of vegetation driving factors and mining-induced quantification in the Fengfeng District, China. Ecol. Inform. 80, 102506. https://doi.org/10.1016/j.ecoinf.2024.102506.
Zhao, Y., Lu, M., Chen, D., Zhang, L., 2024. Understanding the weakening patterns of inner Tibetan plateau vortices. Environ. Res. Lett. 19 (6), 064076. https://doi.org/10.1088/1748-9326/ad5193.
Zheng, Z., Luo, F., Li, N., Gao, H., Yang, Y., 2024. Impact of local climate zones on the urban heat and Dry Islands in Beijing: spatial heterogeneity and relative contributions. J. Meteorol. Res. 38 (1), 126–137.
Zhou, D., Zhao, S., Zhang, L., Sun, G., Liu, Y., 2015. The footprint of urban heat island effect in China. Sci. Rep. 5. https://doi.org/10.1038/srep11160.
Zhou, D., Xiao, J., Bonafoni, S., Berger, C., Deilami, K., Zhou, Y., Frolking, S., Yao, R., Qiao, Z., & Sobrino, J. A. (2019a). Satellite remote sensing of surface urban heat islands: Progress, challenges, and perspectives. In Remote Sens. (Vol. 11, issue 1). doi:https://doi.org/10.3390/rs11010048.
Zhu, Z. (2019). Science of landsat analysis ready data. In Remote Sens. (Vol. 11, issue 18). doi:https://doi.org/10.3390/rs11182166.
Zhu, Z., Fu, Y., Woodcock, C.E., Olofsson, P., Vogelmann, J.E., Holden, C., Wang, M., Dai, S., Yu, Y., 2016. Including land cover change in analysis of greenness trends using all available Landsat 5, 7, and 8 images: a case study from Guangzhou, China (2000–2014). Remote Sens. Environ. 185. https://doi.org/10.1016/j.rse.2016.03.036.